Development of robust pressure management strategies for geologic CO 2 sequestration

Harp, Dylan Robert
Pawar, Rajesh J.
Stauffer, Philip H.
O'Malley, Daniel
Ziao, Zunsheng
Egenolf, Evan P.
Miller, Terry Ann

To be published in: International Journal of Greenhouse Gas Control

DOI to publisher's version: 10.1016/j.ijggc.2017.06.012

Permalink to record: http://permalink.lanl.gov/object/view?what=info:lanl-repo/lareport/LA-UR-16-28892

Development of Robust Pressure Management Strategies for Geologic CO_2 Sequestration

Dylan R. Harp[a,*], Philip H. Stauffer[a], Daniel O'Malley[a], Zunsheng Jiao[b], Evan P. Egenolf[b], Terry A. Miller[a], Daniella Martinez[a], Kelsey A. Hunter[c], Richard S. Middleton[a], Jeffrey M. Bielicki[c,d], Rajesh Pawar[a]

[a]*Earth and Environmental Sciences Division, Los Alamos National Laboratory, Los Alamos, NM, 87544*
[b]*Carbon Management Institute, University of Wyoming, Laramie, WY, 82072*
[c]*Department of Civil, Environmental, and Geodetic Engineering, The Ohio State University, Columbus, OH, 43210*
[d]*The John Glenn College of Public Affairs, The Ohio State University, Columbus OH 43210*

Abstract

Injecting CO_2 into deep geologic formations for permanent storage can potentially lead to leakage or induced seismicity if the overpressures exceed the fracture gradient or fault re-activation pressure. Strategies that remove reservoir fluids before or after injection may reduce these risks. But, even extensively characterized reservoirs can have substantial gaps in characterization necessary for developing optimal deterministic or even probabilistic pressure management strategies. The characterization data may not provide well-defined bounds or distributions of reservoir parameters or conditions (permeability, fault locations, fracture gradient, fault reactivation pressure). To assess the impact of these uncertainties, we present an approach for evaluating alternative pressure management strategies based on their robustness of meeting project performance criteria. We quantify the robustness of alternative strategies against several criteria: (1) exceeding fault re-activation

*Corresponding author: Dylan R. Harp (dharp@lanl.gov)

pressure, (2) failing to inject a desired quantity of CO_2, (3) exceeding a maximum quantity of extracted brine, and (4) failing to reach a desired extraction efficiency. Our approach allows nuances of competing and complimentary criteria to be quantitatively evaluated in a manner and in a level of detail not possible with optimization approaches. We illustrate the fundamentals of the approach on a simple one-dimensional analytical example using the Thiem equation. We demonstrate the approach using a numerical flow and transport model with uncertain heterogeneous permeabilities using data and site characteristics from the Rock Springs Uplift Carbon Storage Site in southwestern Wyoming.

Keywords: pressure management, decision analysis, brine extraction, robustness

1. Introduction

Efforts to sequester CO_2 from the atmosphere by injection into deep subsurface formations will result in overpressurization of target reservoirs. Successful pressure management strategies during CO_2 sequestration (Viswanathan et al., 2008; Benson and Cole, 2008; Birkholzer and Zhou, 2009; Stauffer et al., 2011; Middleton et al., 2012) operations can be used to protect the integrity of overlying caprock and nearby faults. Failure to accomplish these goals through pressure management could result in: leakage of CO_2 to shallow aquifers leading to potential contamination of water resources (Keating et al., 2010; Little and Jackson, 2010; Trautz et al., 2012; Navarre-Sitchler et al., 2013; Bacon et al., 2016; Keating et al., 2016); leakage of CO_2 to the atmosphere, i.e., failure of the intent of the operation (Lewicki et al., 2007a,b); induced seismicity (Sminchak et al., 2002; Lucier et al., 2006; Cappa and Rutqvist, 2011; Dempsey et al., 2014), leakage along abandoned wells (Watson et al., 2007; Nordbotten et al., 2008; Pruess, 2008; Carey et al., 2010; Huerta et al., 2012; Jordan et al., 2015; Harp et al., 2016), interaction with other subsurface resources (Bielicki et al., 2014), deterioration of policy and/or public support (Palmgren et al., 2004; Curry et al., 2005; Miller et al., 2007; Wilson et al., 2008; Elliot et al., 2012), and economic costs and financial risk that could be obstacles to deployment (Bielicki et al., 2016).

Proposed geologic CO_2 sequestration (GCS) operations may be placed under scrutiny by association with recent, controversial subsurface energy-related operations, such as: (1) shallow aquifer methane contamination associated with hydraulic fracturing during directional-drilling natural-gas extraction (Osborn et al., 2011; Davies, 2011; EPA, 2016); (2) seismic activity induced by wastewater injection (Ellsworth, 2013; Keranen et al., 2014) and enhanced geothermal systems energy development (Majer et al., 2007; Giardini, 2009; Mukuhira et al., 2013). Therefore, the effectiveness of pressure management strategies must be demonstrated to not just be optimal with respect to cost, but also robust against failure.

Pressure management will primarily include decisions regarding the locations of injection and extraction wells and injection and extraction schedules. Buscheck et al. (2011) investigated “active” pressure management strategies using a 2D radial model progressively moving the radial extraction zone away from the CO_2 injection well. They demonstrated numerically that active pressure management effectively reduced reservoir overpressures and the area of caprock exposed to CO_2, resulted in less aqueous-phase

CO_2 leakage through the caprock seal, and enabled larger volumes of CO_2 to be injected. They also concluded that delaying extraction operations did not significantly impact the reduction in overpressure and that effective pressure management could be accomplished with relatively few extraction wells placed far from the CO_2 injection well. Their research indicates that pressure management may have benefits beyond purely reducing overpressures in storage reservoirs by increasing CO_2 injection volumes.

Buscheck et al. (2016a,b) proposed pre-injection brine extraction at CO_2 injection wells to create initially under-pressurized reservoir conditions to facilitate pressure management. This approach has the added benefit that if extraction is the mirror image of injection at a well, reservoir storage capacity and compartmentalization can be analyzed prior to CO_2 injection.

Birkholzer et al. (2012) proposed an optimal pressure management strategy focused on high impact locations, such as fault zones. They demonstrate that extraction ratios (defined as the extracted volume of brine divided by the injected CO_2 volume) can be reduced significantly by placing extraction wells near high impact features. They propose using automated model inversion to minimize extraction volumes to meet overpressure thresholds at known high impact locations.

What is missing from current pressure management strategy selection is consideration of the robustness of alternative strategies given the inherent uncertainties in GCS site characterization and operations (reservoir permeability, compartmentalization, fault locations and sealing capacities, etc.). Considering the robustness of meeting performance criteria, given alternative strategies, is important for applications that involve sparse and/or indirect observations (e.g., deep subsurface energy extraction and storage applications). Pressure management strategy selection based solely on cost optimization will drive the decisions to strategies that exactly meet one or more operational criteria. These approaches are attractive because they can lead to a single decision, but a pressure management strategy selection process that considers the risk of failure will result in a more nuanced decision making process and will ultimately lead to better informed decisions.

We describe a pressure management decision analysis, based on concepts from information gap theory (Ben-Haim, 2006), that quantifies the immunity from failure, or robustness, of alternative pressure management decisions. In this paper, we characterize the robustness as the immunity from the following failures: (1) reactivation of an existing fault, (2) failing to inject a desired quantity of CO_2, (3) extracting more brine than anticipated, and (4) the brine extraction operation failing to result in a desired increase in CO_2 injection volume. In our analysis, we assume that the extracted brine will be treated as opposed to re-injected. Therefore, we do not consider the risks associated with re-injection, but use the quantity of brine extracted as a proxy for the cost of treatment. The approach can be applied to cases where there are significant gaps in information precluding probabilistic estimations of parameter distributions, a common situation in deep subsurface applications. The approach could be integrated with probabilistic uncertainty analysis in cases where a combination of probabilistic and non-probabilistic information are available as described by O'Malley and Vesselinov (2015).

We demonstrate the approach on the Rock Springs Uplift Carbon Storage Site (RSUCSS) in southwestern Wyoming (Surdam and Jiao, 2007). Considerable effort has been invested to characterize and understand the RSUCSS, including extensive analyses on a single exploratory well (RSU #1) and geophysical surveys (Surdam, 2013). Stauffer et al. (2009) and Deng et al. (2012) explored the potential for using the RSUCSS for CO_2 sequestration by performing simulations of CO_2 injection into its heterogeneous formations. The information from these efforts provide reasonable nominal model parameters to characterize the reservoir. For example, the analysis of well logs, core, and 3D seismic survey provide a nominal heterogeneous permeability field. This nominal permeability field currently is the best information available to use in CO_2 injection simulations to inform the selection of a pressure management strategy.

A probabilistic characterization of the permeability field in this case would be ill-defined because the only source of spatially-distributed information is from the 3D seismic survey, which is an indirect source of information with a high degree of interpretation, based on permeability/porosity relationships derived well logs and core samples. In fact, the only direct estimates of permeability for the target reservoir are from RSU #1 core samples. A probabilistic pressure management strategy decision analysis (i.e., based on Bayesian decision theory (Berger, 2013)) would require the specification of prior probabilistic distributions of parameters (e.g., parameters defining the spatial distribution of permeabilities), which is not warranted given the available information. A robust Bayesian analysis (Berger et al., 1994) would explore the sensitivity of alternative priors, but it would require a set of Bayesian analyses, each with significant computational requirements, without eliminating the need for probabilistic assumptions. The approach we present provides a quantitative analysis of the relative robustness of pressure management strategies against failure without requiring probabilistic assumptions about uncertain parameter distributions. We focus on the uncertainty/lack of information regarding the permeability field in our analysis since it will have a dominant impact on the robustness of the pressure management strategy against induced seismicity along existing faults. It is also often the least known parameter. It is possible to evaluate uncertainties associated with other parameters, or multiple parameters, lacking in information in a similar manner.

Background on the strategy selection approach is provided in Section 2. To illustrate fundamentals, we provide a simple analytical example allowing the analysis to be demonstrated using closed-form equations (Section 2.1). In the Methods Section (Section 3), we describe the RSUCSS data and numerical model (Section 3.1) and the strategy selection process applied to the RSUCSS (Section 3.2). In the Results Section (Section 4), we present robustness analyses for (1) single passive extraction wells comparing different locations between the CO_2 injection well and the fault (Section 4.1), (2) single passive extraction wells comparing different quantities of pre-injection brine extraction volumes (Section 4.2), (3) three sequential passive extraction wells stepping back from the CO_2 injection well towards the fault as breakthrough occurs comparing different brine extraction well locations (Section 4.3), (4) three sequential passive extraction wells comparing different pre-injection brine extraction volumes (Section 4.4), (5) single extraction well actively produced comparing different constant extraction rates

(Section 4.5), and (6) single extraction well actively produced with constant rate extraction comparing different quantities of pre-injection brine extraction (Section 4.6). In the Discussion Section (Section 5), we demonstrate how the robustness analyses can be used to select a pressure management strategy based on desired performance criteria.

2. Background on approach

Information gap decision theory is a non-probabilistic approach for quantifying the robustness of alternative decisions in situations where significant gaps in information exist. In contrast to distribution-based (probabilistic) methods, it is set based. Uncertainty models in information gap decision theory identify nested sets of parameter value combinations around nominal parameter values. The nominal parameter values are the current best estimates that would be used to make a decision today. For example, in the RSUCSS example, the nominal parameter values are the derived permeabilities of the target reservoir. The main outcome of an information gap decision analysis is a metric of robustness, where robustness quantifies *the degree that we can be incorrect in our characterization of the system and still ensure that performance criteria are met.* Strategy selection approaches based on optimization do not directly address robustness, instead focusing on optimizing operational decisions (e.g., well placement, injection and extraction schedules) to exactly meet performance criteria, thus ignoring the effect of uncertainties on strategy robustness. In the RSUCSS example, the system characterization would be the reservoir permeability field and the performance criteria would be to (1) not overpressurize a known fault (the

Jim Bridger Fault), (2) inject a desired quantity of CO_2, (3) not exceed a specified quantify of brine extraction, and (4) achieve a desired extraction efficiency.

In order to illustrate the fundamentals of our approach, in the following section we consider a simple model allowing the analytical derivation of a pressure management robustness metric. A slightly more complex analytical example of information gap decision theory based on an analytical solution of two-dimensional advective-dispersive transport is presented in Harp and Vesselinov (2013). Additionally, Ben-Haim (2006) contains numerous analytical illustrations of information gap decision theory across a wide range of applications.

2.1. Simple analytical decision analysis demonstration

We will use a steady-state, single (water) phase, one dimensional model based on the Thiem equation (Thiem, 1906)to simulate the overpressure at a sealing fault,

$$\mathrm{d}p(Q_p) = \frac{\rho g}{\pi k b}\left[Q_i \ln\frac{x_f}{R} - Q_p \ln\frac{x_f - x_p}{R}\right] \tag{1}$$

where the CO_2 injection well is located at the origin ($x = 0$), x_f is the location of the fault, x_p is the location of the brine extraction well, ρ is the density of water, g is the acceleration due to gravity, k is the permeability, b is the thickness of the confined reservoir where injection/extraction is taking place, Q_i is the injection rate, Q_p is the extraction rate, and $R \gg x_f$ represents a boundary location where there is approximately no change in pressure. We assume $b = 1000$ m, $x_f = 1000$ m, $x_p = 800$ m, $Q_i =$

$0.01\ \mathrm{m}^3/\mathrm{s}$, and $R = 100$ km. The permeability of the formation is uncertain, but nominally considered to be $k = 10^{-10}\ \mathrm{m}^2$. The decision to be made is to choose a value for Q_p that keeps $\mathrm{d}p(x_f)$ below a desired threshold (i.e., is robust against overpressurizing the fault) while being robust against uncertainty in k. This simple decision analysis is meant only to demonstrate the methodology in a closed-form analytical framework. While the use of a single-phase solution is an idealization, it has been demonstrated that it is reasonable for small pressure increases far from the injector (Nicot et al., 2011). A practical example is considered in the remainder of the paper.

We define the uncertainty model

$$U_m(h) = \left\{m_k : |m_k| \leq h\right\}, h \geq 0 \tag{2}$$

where m_k is a permeability modifier that is used to increase or decrease the permeability as

$$k_m = 10^{\log_{10}(k)+m_k}. \tag{3}$$

As h increases, the possible values of m_k included in set U_m increases, thereby increasing the set of permeability values (k_m) that can be considered.

For a given overpressurization threshold, $\mathrm{d}p_f^c$, we define the robustness of an extraction rate, Q_p, as

$$\hat{h}(\mathrm{d}p_f^c, Q_p) = \max\left\{h : \max_{m_k \in U_m(h)} \mathrm{d}p(Q_p) \leq \mathrm{d}p_f^c\right\} \tag{4}$$

Equation 4 locates the maximum absolute value that m_k can deviate from nominal ($h = 0$) and still meet the performance criterion that $\mathrm{d}p(Q_p) \leq \mathrm{d}p_f^c$. In other words, for a given Q_p, how incorrect can we be in our nominal permeability and still meet our performance criterion.

Substituting equation 3 for k in equation 1 and solving the inequality in equation 4 for m_k, it follows that

$$\hat{h}(\mathrm{d}p_f^c, Q_p) = \max\left\{0, -\log_{10}\left[\frac{\rho g}{\pi k b \mathrm{d}p_f^c}\left(Q_p \ln\frac{x_f - x_p}{R} - Q_i \ln\frac{x_f}{R}\right)\right]\right\} \tag{5}$$

This equation is valid when $Q_p < Q_i \frac{\ln\frac{x_f}{R}}{\ln\frac{x_f - x_p}{R}}$, as is the case in our analysis, which ensures that values less than or equal to zero are not introduced as arguments of the logarithmic function.

Figure 1 shows the robustness (equation 5) as a function of the overpressurization threshold ($\mathrm{d}p_f^c$) for three extraction rates (Q_p). For a given overpressurization threshold, increasing the extraction rate also increases robustness. In this scenario, an operator must choose a balance between increased robustness against uncertainty in the permeability and the increased cost from pumping and treating higher flow rates of brine that comes with a higher extraction rate. For example, if $\mathrm{d}p_f^c$ is deemed to be 30 Pa, there is an increase in robustness of around 1 by increasing the extraction rate from 0.0073 to 0.0074 m^3/s, which means that by choosing the higher rate, we can be 1 order of magnitude more incorrect in our nominal concept of the reservoir permeability and still not exceed our fault overpressure threshold. As discussed above, this increase in robustness will come at the price of increased pumping and treatment costs.

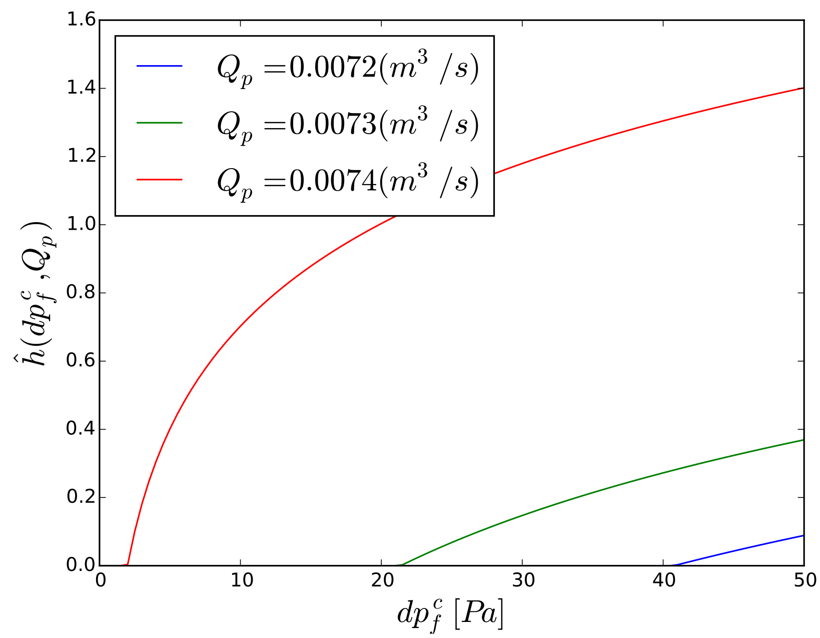

Figure 1: The robustness to uncertainty in the reservoir permeability for three extraction rates. For a given overpressurization threshold, increasing the extraction rate results in increased robustness.

This approach differs from optimization approaches, which would formulate the problem as

$$\text{minimize } Q_p \text{ such that } \mathrm{d}p(Q_p) \leq \mathrm{d}p_f^c. \tag{6}$$

Performing this optimization for a designated value of $\mathrm{d}p_f^c$ will identify the value of Q_p with zero robustness. In Figure 1, this corresponds to solutions along the x-axis where $\hat{h} = 0$. A detailed analysis of performance robustness would not be provided by solving equation 6 since only the trajectory of the optimization would be evaluated.

3. Methods

3.1. Site description and numerical model development

The Wyoming State Geological Survey has identified the region around the Jim Bridger Power Plant (i.e., the RSUCSS) as the premier CO_2 storage site in Wyoming (Surdam and Jiao, 2007). The Jim Bridger Power Plant produces up to 18 Mt of CO_2 per year, providing an abundant local source of CO_2 that could be captured for geologic storage in the RSUCSS. Surdam et al. (2009) identified the likely need for brine production to reduce reservoir overpressure and increase storage capacity during large-scale CO_2 injection at the site.

Additional work undertaken jointly with the US Department of Energy (DOE) as part of the Wyoming Carbon Underground Storage Project (WY-CUSP) has generated high resolution data from the RSUCSS (Surdam, 2013). The stratigraphy of the RSUCSS is believed to contain many competent sealing units above the Madison Limestone formation to contain the buoyant CO_2 (Figure 2). The exploratory well RSU #1 provides the most detailed information at the site, and is used as the location of the CO_2 injection well in this study. 3D seismic surveys, well logs, and core analysis indicate that the Upper Madison has significantly lower porosities and permeabilities than the Lower Madison (Figure 3). We therefore focus on the Lower Madison as the target CO_2 storage reservoir in this study. While the level of compartmentalization of the Madison is uncertain, the existence of the Jim Bridger Fault approximately 2 km to the northeast is believed to be known with a high degree of certainty from the available seismic and well logs.

The interpretation of 3D seismic survey, well logs, and cores (Surdam, 2013, Chapters 6 and 7) informed the development of a Finite Element Heat and Mass Transfer (FEHM; https://fehm.lanl.gov) numerical model. The computational mesh, developed using the Los Alamos Grid Toolbox (LaGriT; http://lagrit.lanl.gov), conforms with interfaces of the stratigraphic layers present at the RSUCSS (top image in Figure 4) . The computational mesh is centered on the RSU #1 well with approximate lateral extents of 6 by 6 km and from 2.8 to 4.3 km below the ground surface. The mesh conforms to formation interfaces between the Darby, Lower Madison, Upper Madison, Amsden, and Weber formations, although heterogeneous porosities and permeabilities are only applied to the Lower Madison. Since permeabilities will be the dominant control on overpressure along the Jim Bridger Fault, they are the focus of our analysis, while the heterogeneous porosity field is fixed. The top image in Figure 4 displays the mesh connectivity where the

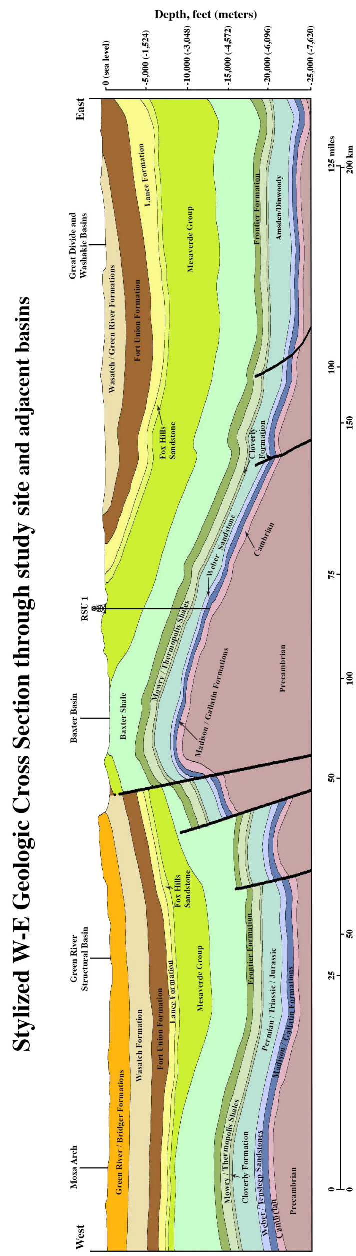

Figure 2: Stylized cross section across the RSU and adjacent sub-basins showing the position of the RSU #1 well (modified from Clarey and Thompson (2010)).

vertical resolution varies between 9.4 m in the Upper Madison and 8.7 m in the Lower Madison. The uniform lateral resolution of the mesh is 67 m.

The center and bottom images in Figure 4 display the derived permeability field in side and plan view. Chapter 9 of Surdam (2013) describes details of the derivation of the porosity/permeability relationships used to calculate the permeabilities from porosities derived from the 3D seismic survey. Based on analysis of well logs and interpretation seismic surveys, the Upper Madison is considered to be a potential upper seal on the Lower Madison and is modeled with low uniform permeability (1×10^{-18} m^2; 0.001 mD), as are the other formations.

The FEHM model includes the Jim Bridger Fault, located approximately 2 km northeast of RSU #1. Since the Madison is believed to be highly compartmentalized, the lateral boundaries of the model (i.e., boundary conditions), including the Jim Bridger Fault, are modeled as closed boundaries. The assumption that the Jim Bridger Fault is a closed boundary, and therefore does not conduct any pressure, is a conservative assumption. If the Jim Bridger Fault were to conduct pressure, the overpressures would be reduced.

Pressures are initialized within the FEHM model using hydrostatic pressures and atmospheric surface pressure (0.101 MPa). Temperatures are initialized within the FEHM model based on a geothermal gradient of 25.5 °C/km and an average surface temperature of 4.4 °C, which produces temperatures which are consistent with observations in the RSU #1 well.

The fracture gradient at the RSUCSS is estimated by the Carbon Management Institute to be around 13.6 kPa/m (0.6 psi/ft). The initial pressure at the location of the CO_2 injection well (RSU #1) is 37 MPa. Therefore,

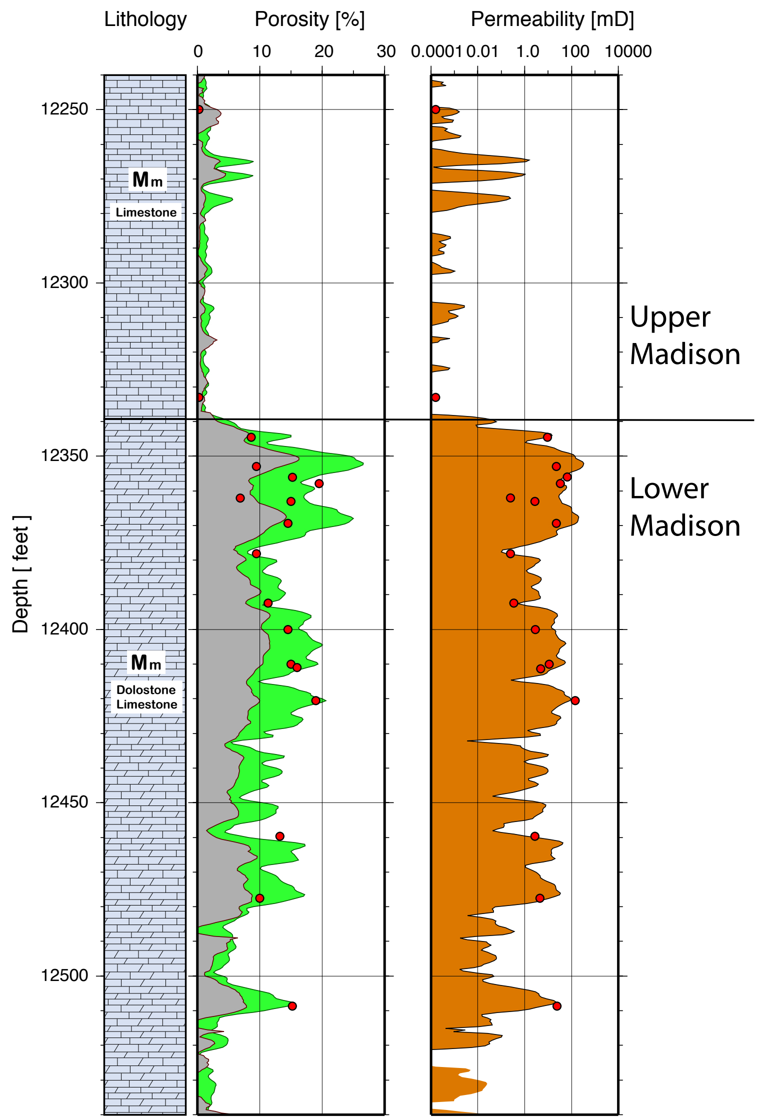

Figure 3: Open-hole logs and core data in the Madison Formation in the RSU #1 well. Tracks from left to right are (1) lithology, (2) density (green) and sonic (gray) porosity with total porosities from core (red dots), (3) permeability from logs (orange) overlaid with core measurements (red dots). The approximate delineation between Upper and Lower Madison formations is indicated on the right. Modified from Figure 9.3 in Surdam (2013).

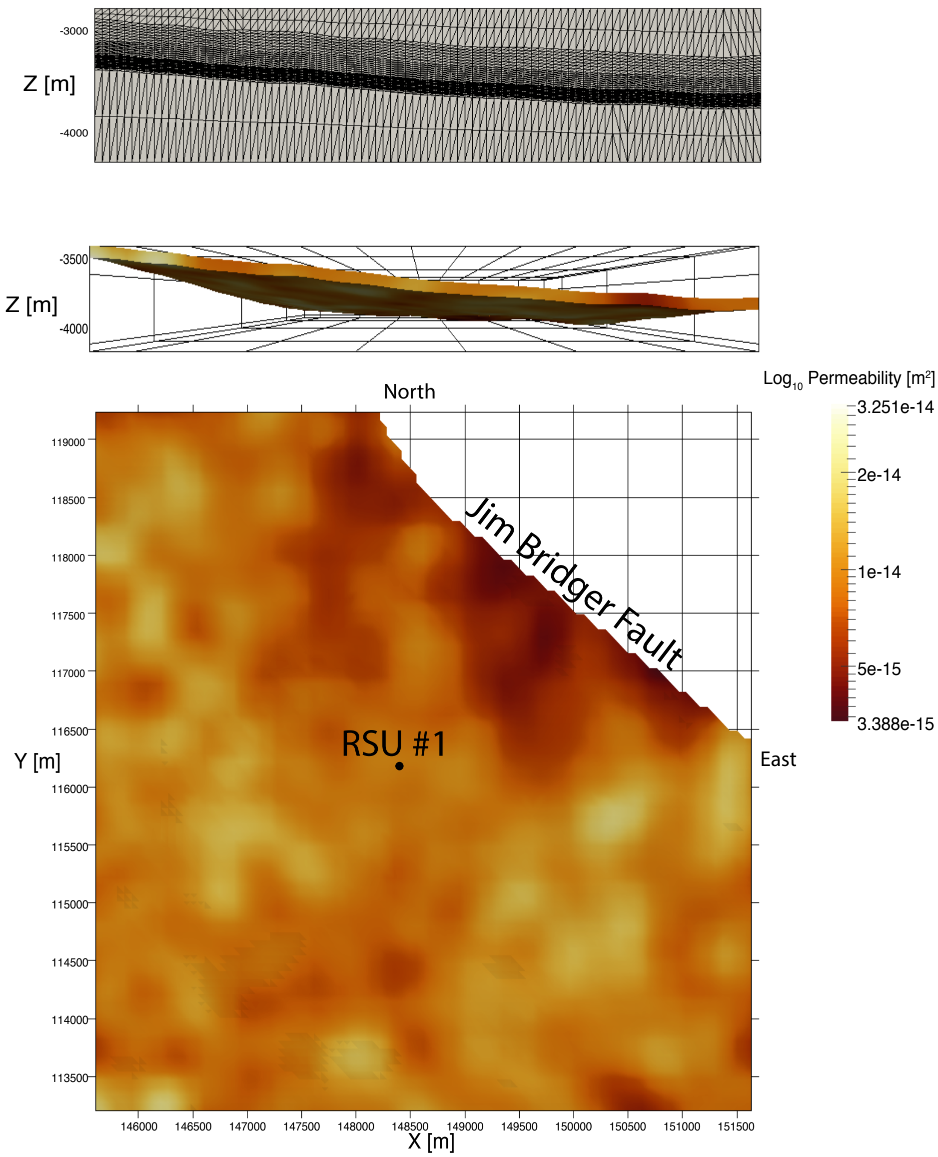

Figure 4: A mesh side view is shown in the top image. Side and map views of Lower Madison derived permeabilities are shown in the middle and bottom images. Axes are in the SPCS27-4903 coordinate system where X increases towards the east, Y increases towards the north. The Z-axis is depth. The location of the Jim Bridger Fault and RSU #1 well are identified in the top view (bottom image). The Jim Bridger Fault is assumed to be a sealing fault in the analysis, so the area to the northeast of the fault is not included in the model.

the caprock fracture pressure at the CO_2 injection well is around 90 MPa. To ensure that CO_2 injection does not cause pressures to exceed the fracture gradient, we begin the injection at a constant rate of 1 Mt/y (31.7 kg/s) until the pressure at the CO_2 injection well reaches 75 MPa (83% of the fracture pressure), and then switch to a constant pressure injection of 75 MPa. Some simulations do not reach 75 MPa at the CO_2 injection well and remain at constant rate injection for their duration.

Single- and triple-extraction well pressure management strategies are investigated here. As described above, the simulation starts with constant injection rate (1 Mt/y) and switches to constant pressure injection if and when pressure at the CO_2 injection well reaches 75 MPa. The simulation is terminated when CO_2 saturation at the brine extraction well exceeds 0.001 (0.1% CO_2). This represents a scenario where the brine extraction wells are effectively turned off immediately after there is breakthrough of the CO_2 plume. Since brine extraction occurs along the bottom of the Lower Madison in our simulations, higher CO_2 saturations may exist along the top of the formation at the location of the brine extraction well prior to terminating the simulation. The triple-extraction well strategy is more complicated because brine extraction switches to another well when CO_2 breaks through. The sequence of operating decisions that are made during triple-extraction well strategies is provided in a flow diagram in Figure S1 in Supplemental material.

In order to show results of the FEHM simulations, we present plots of overpressure contours and CO_2 plume extent during a triple-extraction well simulation in Figure 5. The overpressure contours indicate how the extraction wells reduce pressure at the Jim Bridger Fault. For example, in the final plot at 9.08 years, most of the model boundaries are above 16 MPa, while the Jim Bridger Fault is at 15 MPa near the fault intersection with the boundaries of the mesh and less than 13 MPa closest to the third extraction well. The CO_2 plume is pulled towards the extraction wells. Pulling the CO_2 plume towards extraction wells is a side effect of pressure management and may reduce sweep efficiency of the CO_2 injection operation. A movie that contains the plots in Figure 5 and more effectively illustrates the simulation is provided in the supplementary material.

3.2. Pressure management decision analysis formulation

In this section, we describe the pressure-management strategy selection approach applied to the RSUCSS. While the approach is similar to the analytical example in Section 2.1, it is much more complicated as it involves ensembles of numerical simulations, multiple performance criteria, and cannot be easily described using closed-form equations.

We consider the uncertainty associated with the derived permeabilities of the Lower Madison. Similar to the analytical example, a modifier, m_k, that translates the heterogeneous permeability field by orders of magnitude parameterizes this uncertainty as

$$k_m(\mathbf{x}) = 10^{\log_{10}(k(\mathbf{x}))+m_k}, \tag{7}$$

where k is the derived permeabilities, k_m is the modified permeabilities, and $\mathbf{x}$ represents vector locations within the Lower Madison.

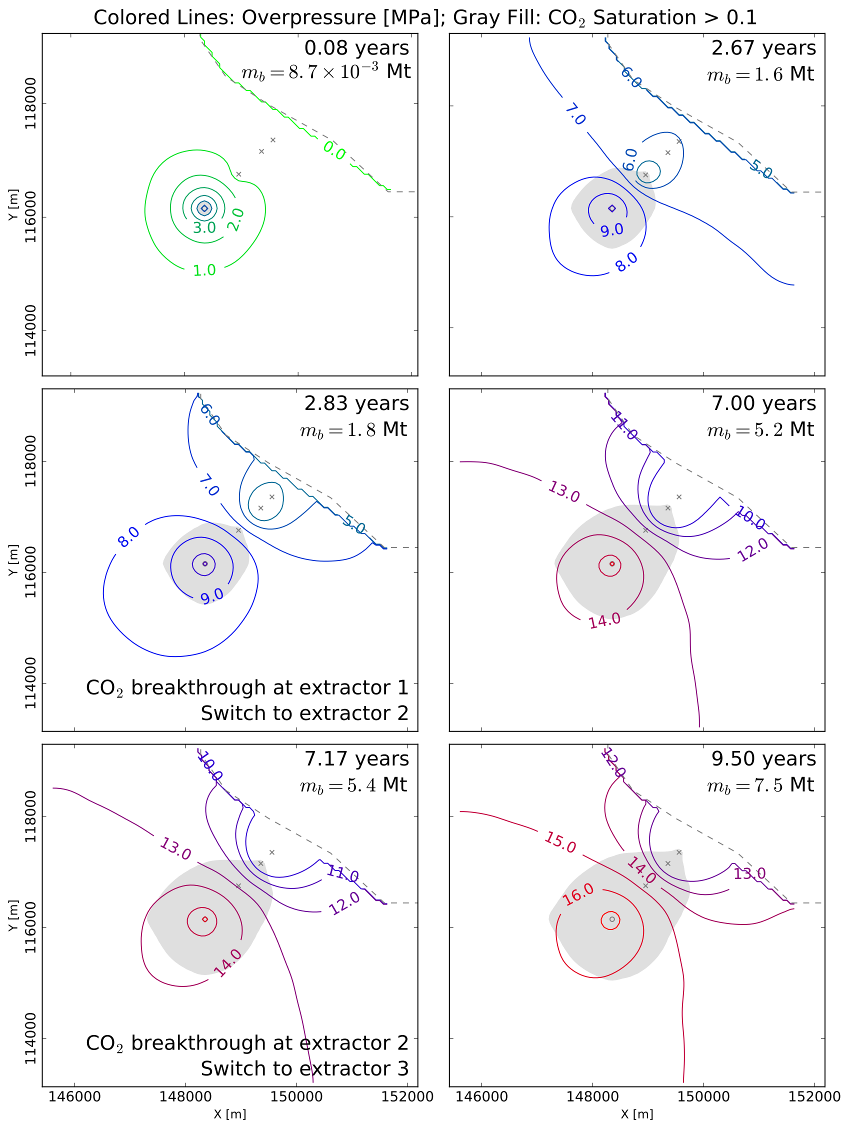

Figure 5: Plan view of overpressure contours (colored lines) and CO_2 plume extent (gray fill) for a triple-extraction well pressure management FEHM simulation. The CO_2 injection well (RSU #1) is indicated by a circle, brine extraction wells are indicated by x's, and the Jim Bridger Fault by a dashed line. The time and cumulative brine extracted (m_b) are indicated in the upper right corner of each plot. Since CO_2 injection is 1 Mt/year, the amount of CO_2 injected in Mt is equal to the time in years. Axes are in the SPCS27-4903 coordinate system.

The nominal value of m_k is zero, since this is the case where permeabilities are not modified from the derived values. We can define our uncertainty model as identical to equation 2 in Section 2.1 using set notation as $U_m(h) = \{m_k : |m_k| \leq h\},\ h \geq 0$.

The performance criteria are to (1) remain below the reactivation overpressure along the Jim Bridger Fault, (2) inject a desired quantity of CO_2, (3) extract a minimal amount of brine, and (4) achieve a desired extraction efficiency. The extraction efficiency quantifies the additional CO_2 that can be injected per unit of brine extracted given the same overpressure at the Jim Bridger Fault.

We define the first criterion as

$$\mathrm{d}p_f < \mathrm{d}p_r^c, \tag{8}$$

where $\mathrm{d}p_f$ is the maximum overpressure along the Jim Bridger Fault ($\max\limits_{\mathbf{x}_f} \mathrm{d}p(\mathbf{x}_f)$), $\mathbf{x}_f$ are vector locations along the Jim Bridger Fault and $\mathrm{d}p_r^c$ is the reactivation overpressure criterion threshold value for the Jim Bridger Fault.

The other three criteria are defined as

$$m_c > m_c^c, \tag{9}$$

$$m_b < m_b^c, \tag{10}$$

and

$$e > e^c, \tag{11}$$

where m is mass, e is extraction efficiency, the subscript c denotes injected

CO_2, the subscript b denotes extracted brine, and superscript c denotes the criterion threshold value.

Using the quantities defined above, the extraction efficiency can be defined as

$$e(\mathrm{d}p_f) = \frac{m_c^e - m_c^n}{m_b} : \mathrm{d}p_f \tag{12}$$

where m_c^e is the mass of CO_2 injected with extraction, m_c^n is the mass of CO_2 injected with no extraction, m_b is the amount of brine extracted, including pre-injection brine extraction if conducted.

We define robustness as we did in Section 2.1 as the amount that the permeability field can be modified from nominal and the performance criteria are still met. The robustness metrics can be defined as (1) the robustness against overpressurizing the Jim Bridger Fault,

$$\hat{h}_{dp} = \max\left\{h : \left(\max_{m_k \in U_m(h)} \mathrm{d}p(\mathbf{x}_f) \leq \mathrm{d}p_r\right)\right\}, \tag{13}$$

(2) robustness against failing to inject a desired quantity of CO_2,

$$\hat{h}_{m_c} = \max\left\{h : \left(\min_{m_k \in U_m(h)} m_c \geq m_c^c\right)\right\}, \tag{14}$$

(3) robustness against extracting more brine than desired,

$$\hat{h}_{m_b} = \max\left\{h : \left(\max_{m_k \in U_m(h)} m_b \leq m_b^c\right)\right\}, \tag{15}$$

and (4) robustness against failing to achieve a desired extraction efficiency,

$$\hat{h}_e = \max\left\{h : \left(\min_{m_k \in U_m(h)} e_c \geq e_c^c\right)\right\}. \tag{16}$$

The inner argument of equations 13 and 15 contain a *max* operator because fault overpressure and brine production are not to exceed a threshold. Conversely, the inner argument of equations 14 and 16 contain a *min* operator since it is desired that CO_2 injection and extraction efficiency at least meet or exceed a threshold.

The overall robustness is defined as the minimum over the individual robustness criteria,

$$\hat{h} = \min\left\{\hat{h}_{dp}, \hat{h}_{m_c}, \hat{h}_{m_b}, \hat{h}_e\right\}. \tag{17}$$

We evaluate equations 13 through 16 by running ensembles of FEHM simulations with various modifications to the nominal permeability field according to equation 2. We provide an example of the effect of the permeability uncertainty on our performance criteria in Figure 6 with plots of an ensemble of criteria values as a function of m_k for the single-extraction well strategy. The criteria given the nominal permeability field are indicated by the dashed vertical line at $m_k = 0$. The effect of deviations from nominal permeabilities on performance criteria are evident as increasing or decreasing criteria values to the left or right of nominal. The information in this figure can be used to evaluate how incorrect our nominal permeability field can be from reality and still meet performance criteria as will be presented

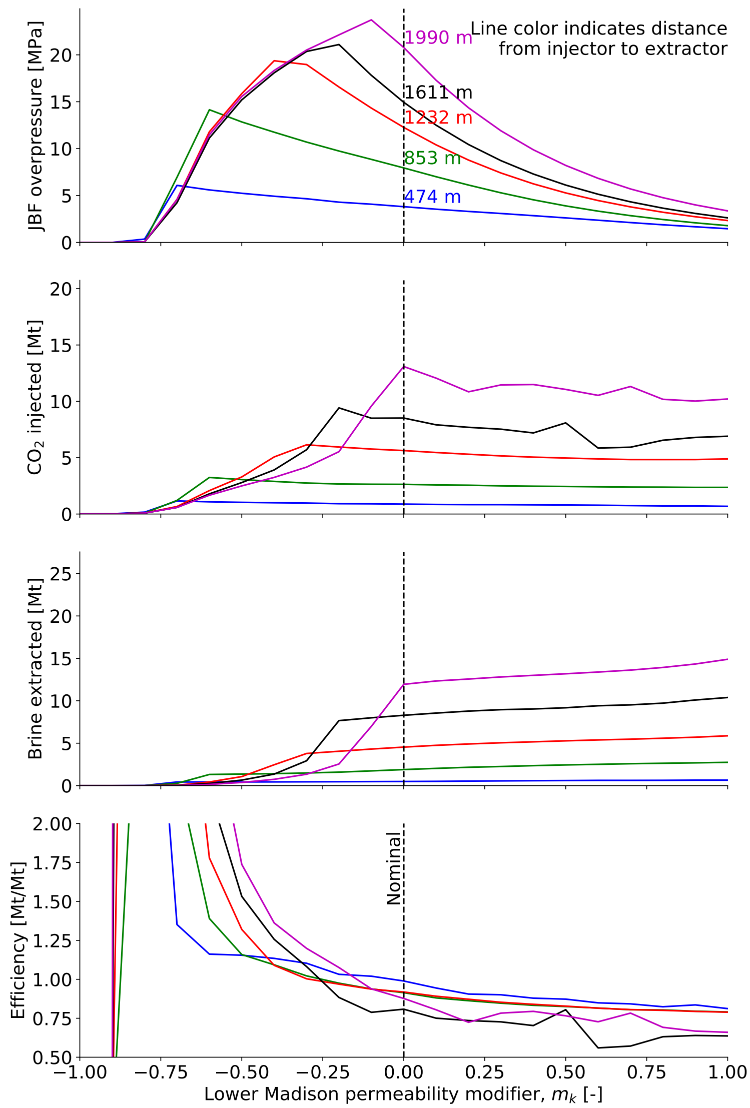

Figure 6: Jim Bridger Fault (JBF) overpressure, CO_2 injected, brine extracted, and extraction efficiency as a function of the permeability modifier for the single-extraction well strategy at different distances from the CO_2 injection well towards the Jim Bridger Fault.

Table 1: Pressure management strategy characteristics for each subsection of the Results section.

Subsection	Single well	Three wells	Pre-injection brine extraction	Passive extraction	Constant rate extraction
4.1	X			X	
4.2	X		X	X	
4.3		X		X	
4.4		X	X	X	
4.5	X				X
4.6	X		X		X

in the Results Section (Section 4).

4. Results

The following subsections contain diagnostic plots for the following strategies: (1) single passive extraction wells comparing different locations between the CO_2 injection well and the fault (Section 4.1); (2) single passive extraction wells comparing different quantities of pre-injection brine extraction (Section 4.2); (3) three sequential passive extraction wells emplaced progressively further from the CO_2 injection well towards the fault as breakthrough occurs comparing different brine extraction well locations (Section 4.3); (4) three sequential passive extraction wells, as described in item 3, comparing different quantities of pre-injection brine extraction (Section 4.4); (5) single extraction well comparing different constant extraction rates (Section 4.5); and (6) single extraction well with constant rate extraction comparing different quantities of pre-injection brine extraction (Section 4.6). Table 1 categorizes the strategies investigated in these subsections.

To show how the performance criteria change over time during CO_2 injection, we present time series plots of overpressure at the Jim Bridger Fault, mass of CO_2 injected, mass of brine extracted, and extraction efficiency (equation 12) for the nominal permeability field as the first figure in the top plot in each subsection (Figures 7, 9, 11, 13, 15, and 17). The overpressure at the Jim Bridger Fault with no brine extraction is shown as a dashed line in each of these figures for reference.

The second figure in each subsection contains plots of robustness as a function of the criteria defined in equations 8 through 11; fault overpressure, CO_2 injection, brine extraction, and extraction efficiency (Figure 8, 10, 12, 14, 16, and 18). Although robustness technically has no upper bound, in our plots, robustness is truncated at a value of 1 because this value was the maximum in the sampling of the permeability modifier; i.e., an order of magnitude above and below nominal. Note that values to the left of this truncation (lower values) for fault overpressure and brine extraction robustness and to the right of this truncation (higher values) for CO_2 injection and extraction efficiency robustness have robustness at least equal to or greater than 1. The ensemble of performance criteria values that form the basis for these robustness plots are presented in Figures 6, S2, S3, S4, S5, and S6, respectively, where the performance criteria are plotted as functions of the permeability modifier (refer to discussion of Figure 6 in Section 3.2).

4.1. Single passive brine extraction well at different locations between the CO_2 injection well and fault

We investigate the results of placing one extraction well at different locations between the CO_2 injection well and the Jim Bridger Fault. In Figure 7, when the extraction well is closer to the injection well, CO_2 breaks through earlier and the extraction well must be shut off. As a result of moving the brine extraction well closer to the fault (farther from the CO_2 injection well), more CO_2 can be injected for storage. This beneficial increase of CO_2 storage results in higher overpressure at the fault. By the end of the simulations, extraction efficiencies for the different locations of the brine extraction wells are slightly increasing with distance, except for the extraction well that is closest to the CO_2 injection well (474 m), where the extraction efficiency is highest.

In Figure 8, when the brine extraction well is closer to the CO_2 injection well, the robustness against fault overpressure, brine extraction, and extraction efficiency are also higher. The sharp increases/decreases in robustness in the plots in Figure 8 are a direct result of changes to criteria values as the magnitude of the permeability modifier increases. For example, for the fault overpressure criterion (top left plot in Figure 8), the robustness for the 474 m case (blue line) is zero up to around 4 MPa, and then increases quickly to a robustness of 1 at around 6 MPa. Looking back at the 474 m case (blue line) in the top plot in Figure 6, the reason for this can be deduced. At the nominal permeability modifier (vertical dashed line at $m_k = 0$), the 474 m case is around 4 MPa, and therefore, there is zero robustness up to 4 MPa. As the permeability modifies decreases (i.e., absolute magnitude included in U_m increases as h in equation 13 increases), the overpressure increases slowly to around 6 MPa, corresponding to the sharp increase in robustness in Figure 8. The 474 m curve for overpressure robustness in Figure 8 is derived directly from the information in Figure 6, as are the curves for the all the other cases and other criteria.

The most robust brine extraction well location is more nuanced and complicated for CO_2 injection as the maximum robustness strategy (top curve) changes as the CO_2 injection criterion value changes. Strategy selection may change if the criterion threshold value is changed. For example, the location with maximum robustness is the *474 m* case if the desired quantity of CO_2 injection is 1 Mt of CO_2, the *853 m* case for 2 Mt CO_2, the *1232 m* case for 4 Mt CO_2, the *1611 m* case for 7 Mt CO_2, and the *1990 m* case for 10 Mt CO_2. Figure 6 contains the performance criteria as a function of permeability modifier, which is the basis for the plots in Figure 8 and equations 13 through 16.

4.2. Single brine extraction well with different quantities of pre-injection brine extraction

We assume a single brine extraction well located at the approximate midpoint between the CO_2 injection well and the Jim Bridger Fault, 1232 m from the CO_2 injection well, and evaluate the effect of pre-injection brine extraction on robustness. We compare pre-injection brine extraction quantities of 0.1 Mt and 1 Mt. The pre-injection brine extraction is simulated using a constant brine extraction rate of 1 Mt/y, therefore, 0.1 Mt and 1 Mt correspond to extracting brine for 1/10 and 1 year, respectively. CO_2 injec-

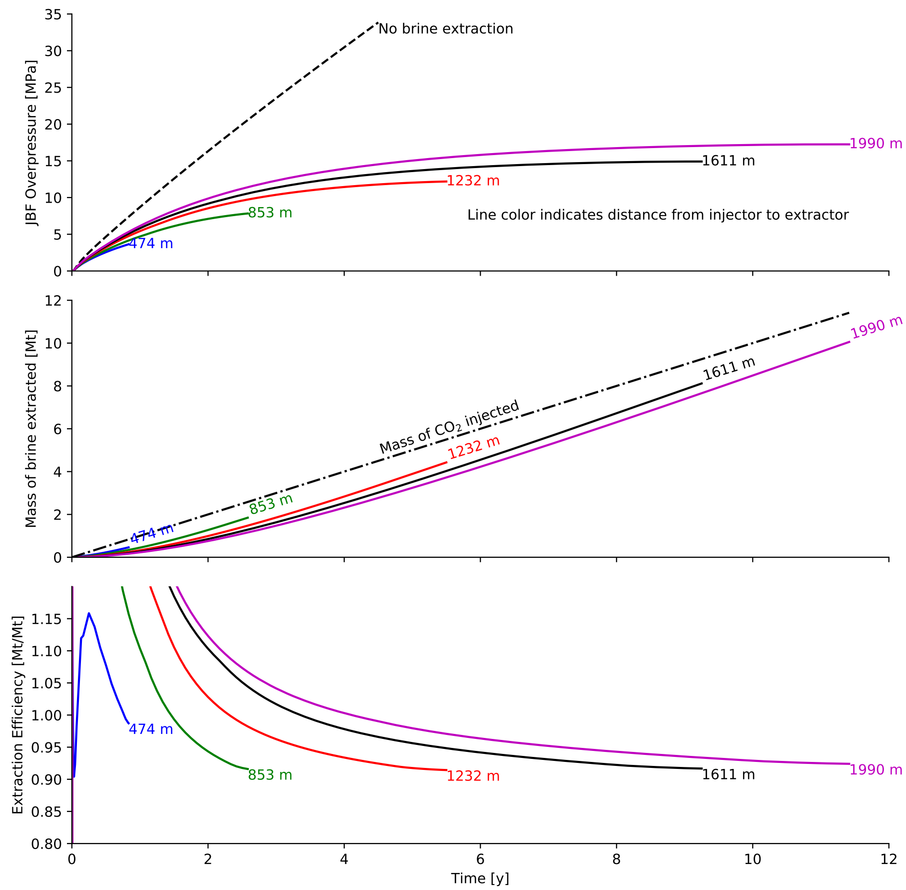

Figure 7: Single brine extraction well strategy with passive brine extraction comparing different distances from the CO_2 injection well towards the Jim Bridger Fault (indicated by line color) for the nominal permeability field. Time series of overpressure at the Jim Bridger Fault (JBF), mass of brine extracted, and extraction efficiency are plotted.

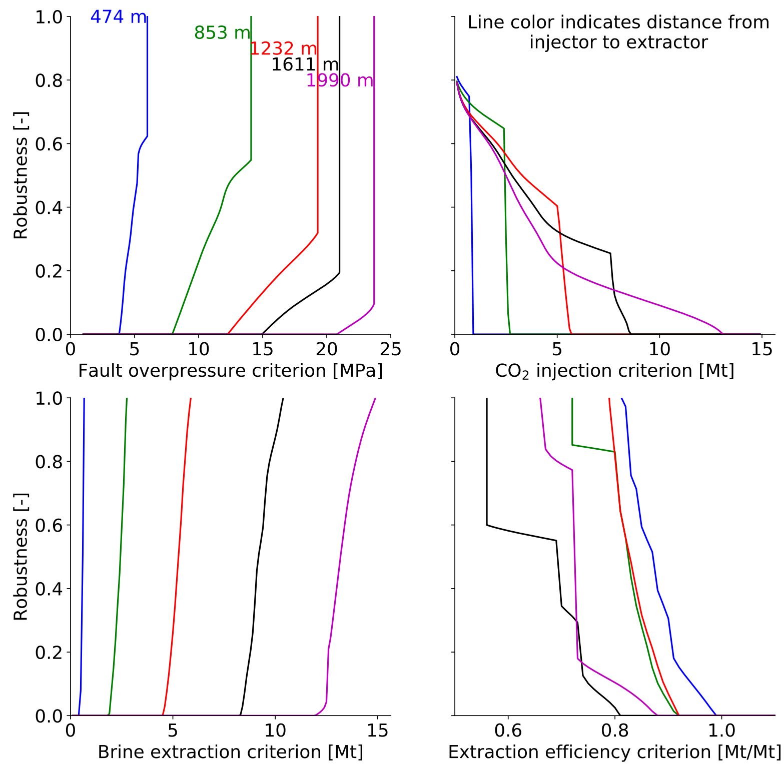

Figure 8: Single brine extraction well strategy with passive brine extraction comparing different distances from the CO_2 injection well towards the Jim Bridger Fault (indicated by line color). Robustness as a function of fault overpressure, CO_2 injection, brine extraction, and extraction efficiency is plotted.

tion simulations are initiated with the final state of the pre-injection brine extraction simulations. The *0 Mt* case is the same as the *1232 m* case in Section 4.1 and is provided for reference.

In the top plot of Figure 9, pre-injection brine extraction delays the onset of fault overpressure. Overpressures resulting from simulations without during-injection brine extraction are presented for each level of pre-injection brine extraction as corresponding colored dashed lines for reference. In the second plot in Figure 9, the initial brine mass at time zero is the pre-injection brine extraction mass (e.g., the *1 Mt* case (red line) begins at 1 Mt at time zero). The extraction efficiencies for the *0.1 Mt* case and *1 Mt* case begin with small values at early times since the mass of brine (denominator of extraction efficiency; m_b in equation 12) begins with non-zero values, as opposed to the *0 Mt* case. The *0.1 Mt* case results in the highest extraction efficiency at the end of the simulations, indicating that more pre-injection brine extraction may not always improve extraction efficiency.

Pre-injection brine extraction of 1 Mt substantially increases the fault overpressure robustness (top left plot in Figure 10). But for the CO_2 injection criteria, the most robust choice depends on the threshold value. The *1 Mt* case has significantly lower brine extraction robustness than the *0 Mt* and *0.1 Mt* cases, which are similar. For extraction efficiency, the *0.1 Mt* case is more robust than the *0 Mt* and *1 Mt* cases, which intersect and cross. Refer to Figure S2 to inspect the ensemble of performance criteria values used as the basis for calculating the robustness metrics in Figure 10.

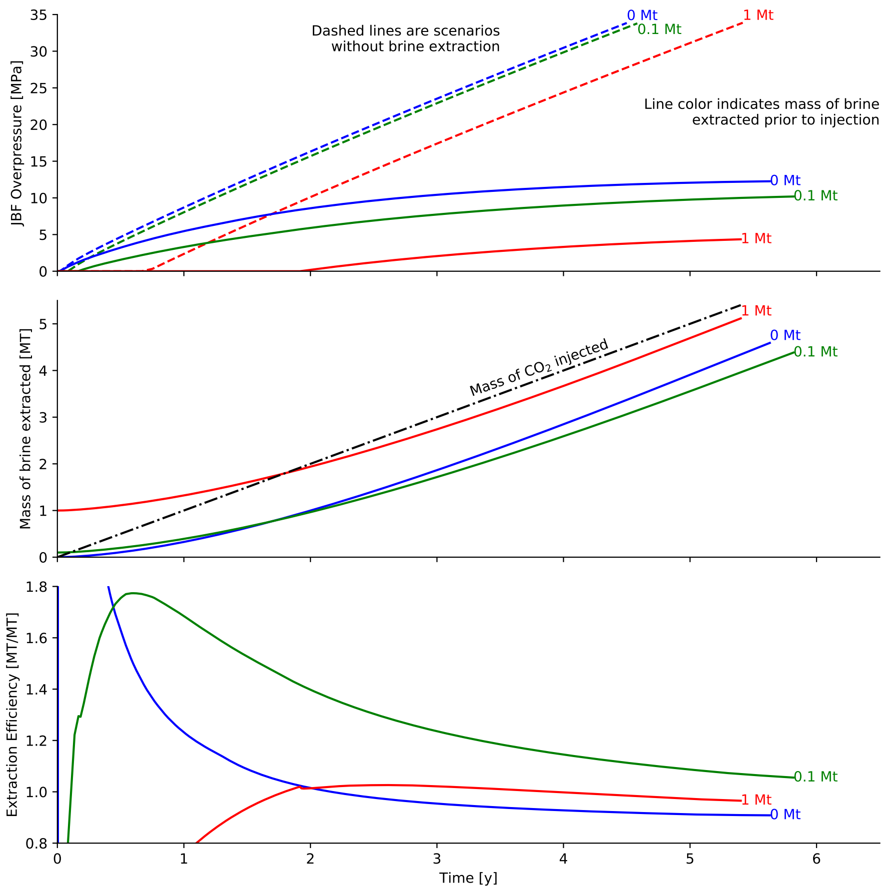

Figure 9: Single brine extraction well strategy with passive brine extraction at 1232 m from the CO_2 injection well comparing different pre-injection brine extraction quantities (indicated by line color) for the nominal permeability field. Time series of overpressure at the Jim Bridger Fault (JBF), mass of brine extracted, and extraction efficiency are plotted.

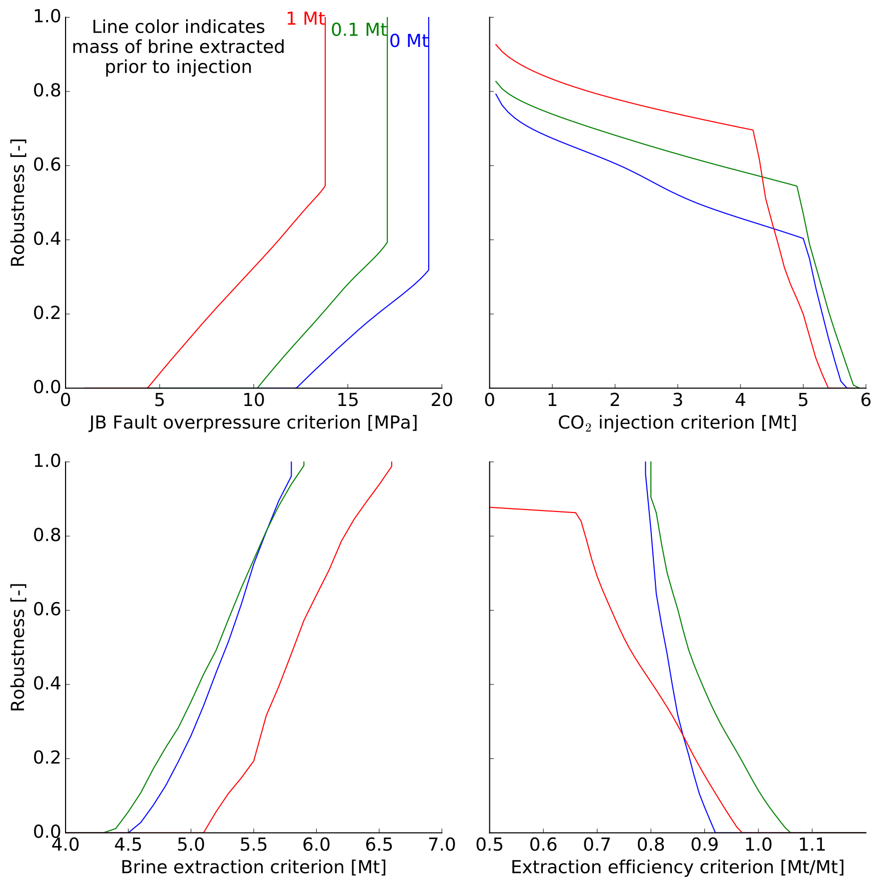

Figure 10: Single brine extraction well strategy with passive brine extraction at 1232 m from the CO_2 injection well comparing different quantities of pre-injection brine extraction (indicated by line color). Robustness as a function of fault overpressure, CO_2 injection, brine extraction, and extraction efficiency is plotted.

4.3. Three sequential passive brine extraction wells starting at different locations between the CO_2 injection well and the fault

We investigate the use of three sequential brine extraction wells located on a line between the CO_2 injection well and the Jim Bridger Fault. Brine extraction successively switches to the next well closer to the fault as CO_2 breakthrough occurs in the operating brine extraction well. We compare three different starting locations for the first brine extraction well, 474, 853, and 1232 m. These distances correspond with computational mesh node locations along a diagonal southwest to northeast line where the diagonal distance between nodes is approximately 95 m. In each case, the next brine extraction well is placed approximately halfway between the existing brine extraction well and the fault. In Figure 11, the slight breaks in the time series (indicated by colored stars) indicate where brine extraction was switched between wells.

According to the robustness plots in Figure 12, placing the first brine extraction well closer to the CO_2 injection well (474 m) leads to greater fault overpressure robustness and brine extraction robustness. CO_2 injection robustness increases by placing the first well closer to the fault (1232 m). Extraction efficiency robustnesses are similar with the first brine extraction well located at 853 m showing higher robustness in general.

In general, closer distance to the CO_2 injection well result in lower fault overpressure, less brine extraction, and less CO_2 injection due to earlier CO_2 breakthrough at the brine extraction wells. Refer to Figure S3 to inspect the ensemble of performance criteria values used as the basis for calculating the robustness metrics in Figure 12.

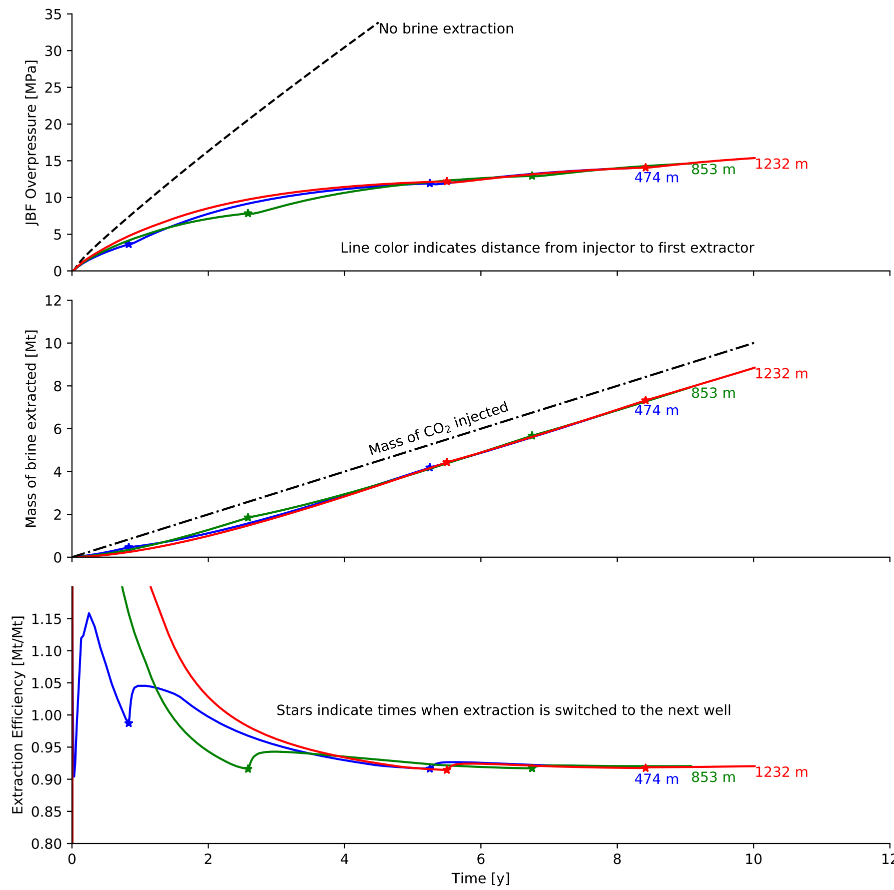

Figure 11: Triple brine extraction well strategy with passive brine extraction comparing different distances from the CO_2 injection well to the first brine extraction well (indicated by line color) for the nominal permeability field. Time series of overpressure at the Jim Bridger Fault (JBF), mass of brine extracted, and extraction efficiency are plotted. In all strategies, the second and third extraction wells are placed halfway between the previous brine extraction well and the Jim Bridger Fault.

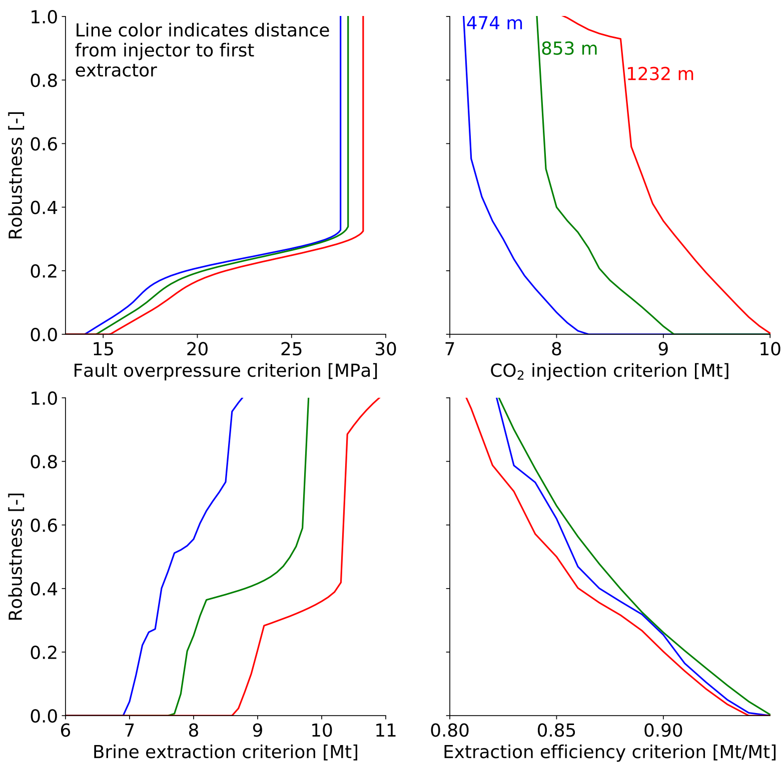

Figure 12: Triple brine extraction well strategy with passive extraction comparing different distances from the CO_2 injection well to the first brine extraction well (indicated by line color). Robustness as a function of fault overpressure, CO_2 injection, brine extraction, and extraction efficiency is plotted.

4.4. Three sequential passive brine extraction wells with different pre-injection brine extraction

We investigate the use of pre-injection brine extraction for the triple brine extraction well strategy placing the first brine extraction well at 853 m from the CO_2 injection well. The *0 Mt* case is the same as the *853 m* case in Section 4.3. The breaks in the time series as brine extraction switches from one well to the next well are indicated by colored stars in Figure 13. As in Figure 9 in Section 4.2, the overpressures resulting from no during-injection brine extraction are presented for each level of pre-injection brine extraction as colored dashed lines and brine mass at time zero includes the mass of pre-injection brine extraction.

In Figure 14, the *1 Mt* case results in higher CO_2 injection robustness, but lower fault overpressure robustness. However, the fault overpressure robustnesses are all similar at around 26 MPa fault overpressure. The results are more complicated for brine extraction efficiency, where the maximum robustness depends on the threshold value with the robustness curves crossing repeatedly. The *1 Mt* case is in general most robust for extraction efficiency, but does have robustness crossover at lower values. Refer to Figure S4 to inspect the ensemble of performance criteria values used as the basis for calculating the robustness metrics in Figure 14.

4.5. Single brine extraction well with different constant brine extraction rates

Up to this point, all of the analyses have used passive brine extraction during CO_2 injection, where the rate of brine extraction adjusts in order to

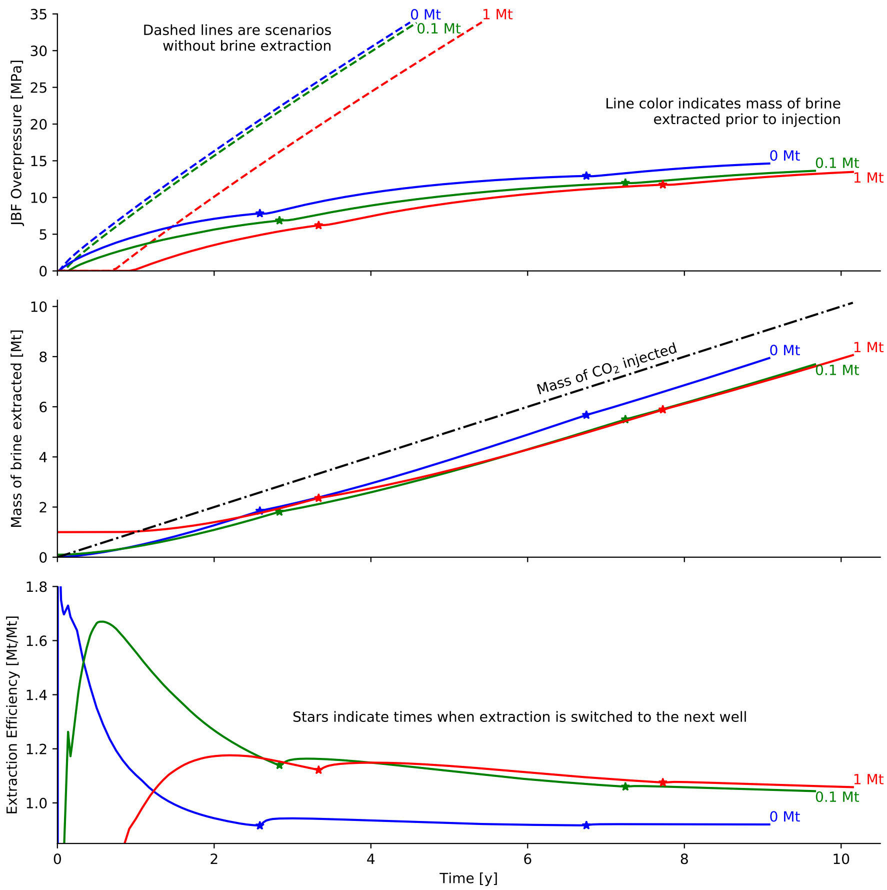

Figure 13: Triple brine extraction well strategy with passive extraction comparing different pre-injection brine extraction quantities (indicated by line color) for the nominal permeability field. Time series of overpressure at the Jim Bridger Fault (JBF), mass of brine extracted, and extraction efficiency are plotted. The first well is located at 853 m from the CO_2 injection well with the second and third well placed halfway between the prior brine extraction well and the Jim Bridger Fault.

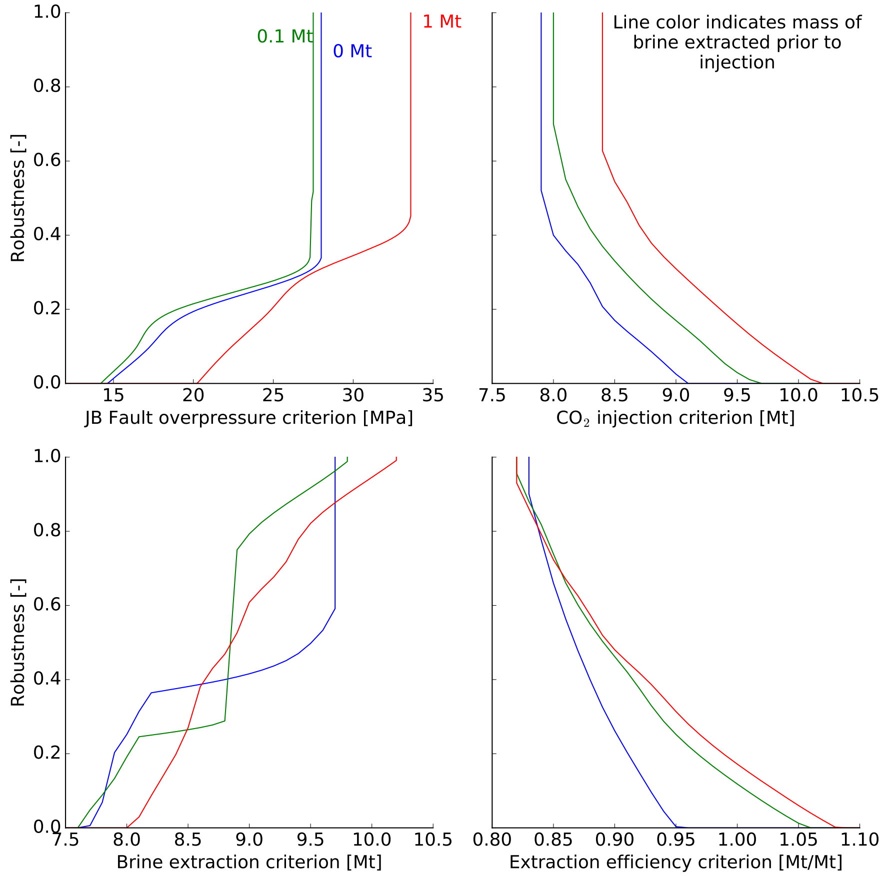

Figure 14: Triple brine extraction well strategy comparing different levels of pre-injection brine extraction (indicated by line color) with the first brine extraction well located at 853 m from the CO_2 injection well. Robustness as a function of fault overpressure, CO_2 injection, brine extraction, and extraction efficiency is plotted.

maintain hydrostatic bottom hole pressure conditions at the brine extraction well. Here we evaluate constant brine extraction rates of 10, 20, and 30 kg/s (approximately 0.32 Mt/y, 0.63 Mt/y, and 0.95 Mt/y). The highest brine extraction rate is close to the constant CO_2 injection rate (1 Mt/y) These brine extraction rates are applied at a single brine extraction well at 1232 m from the CO_2 injection well towards the Jim Bridger Fault.

In Figure 15, as the brine extraction rate increases, the time until overpressure at the fault increases as well. For reference, passive extraction is represented as a gray line in the plots in Figures 15 and 16. The passive strategy is the same as the *1232 m* case in Figures 7 and 8 in Section 4.1. Constant rate extraction leads to a more linear increase in fault overpressure than passive extraction, which increases at a decreasing rate over time as the extraction rate increases to maintain hydrostatic pressure at the point of extraction. The extraction efficiency for constant rate cases converges quickly to constant values over time after the effects of the delayed overpressure response at the fault (effecting the values of m_c^e and m_b for a given $\mathrm{d}p_f$ in equation 12) and slight nonlinearities at early times in the no during-injection brine extraction overpressures dissipate (effecting the value of m_c^n for a given $\mathrm{d}p_f$ in equation 12).

The robustness plots in Figure 16 indicates that highest fault overpressure robustness is achieved with the highest extraction rate (*30 kg/s* case), but that the robustness of CO_2 injection, brine extraction, and extraction efficiency for the *30 kg/s* case is lower. We also note that passive extraction has significantly less brine extraction robustness than constant rate strategies because it results in higher mass of brine extracted (refer to middle plot in Figure 15). Refer to Figure S5 to inspect the ensemble of performance criteria values used as the basis for calculating the robustness metrics in Figure 16.

4.6. Single brine extraction well with constant brine extraction rate comparing different pre-injection brine extraction quantities

Lastly, we evaluate the effects of using pre-injection brine extraction with a constant 20 kg/s brine extraction rate during injection. Comparisons to the corresponding passive extraction scenarios for the 3 levels of pre-injection brine extraction can be made by referring to Figures 9 and 10 in Section 4.2. The *0 Mt* case is the same as the *20 kg/s* case in Figures 15 and 16 in Section 4.5 where we compared different constant brine extraction rates. The mass of brine extraction at time zero includes the pre-injection brine extraction in the middle plot of Figure 17. The *0.1 Mt* extraction case has little effect on criterion robustnesses compared to the 0 Mt case, except for the extraction efficiency robustness, which decreases significantly (Figure 18). The *1 Mt* case has substantially lower overpressure and brine extraction robustness. The *1 Mt* case has approximately equal or less extraction efficiency robustness that the *0.1 Mt* case as well. These results suggests that there are little if any benefits with regard to robustness by combining pre-injection brine extraction with constant-rate brine extraction during CO_2 injection. Refer to Figure S6 to inspect the ensemble of performance criteria values used as the basis for calculating the robustness metrics in Figure 18.

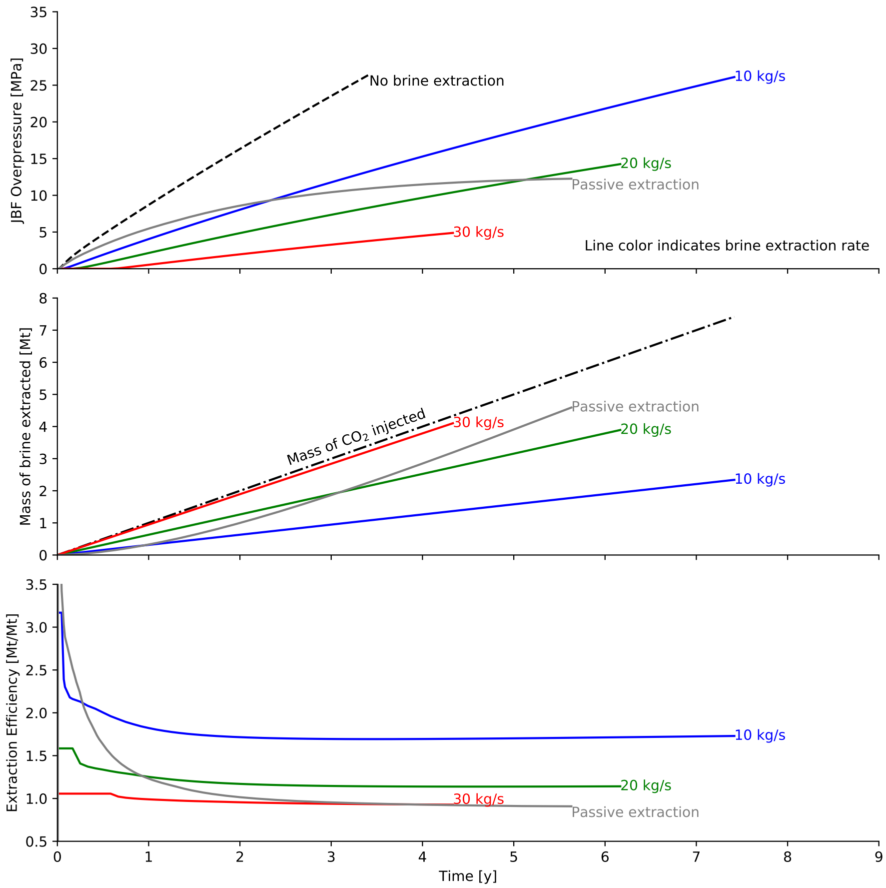

Figure 15: Single brine extraction well strategy comparing different constant brine extraction rates (indicated by line color) for the nominal permeability field. Time series of overpressure at the Jim Bridger Fault (JBF), mass of brine extracted, and extraction efficiency are plotted. The single brine extraction well is located at 1232 m from the CO_2 injection well. The passive extraction scenario at the same well is shown as a gray line and labeled 'Passive extraction'.

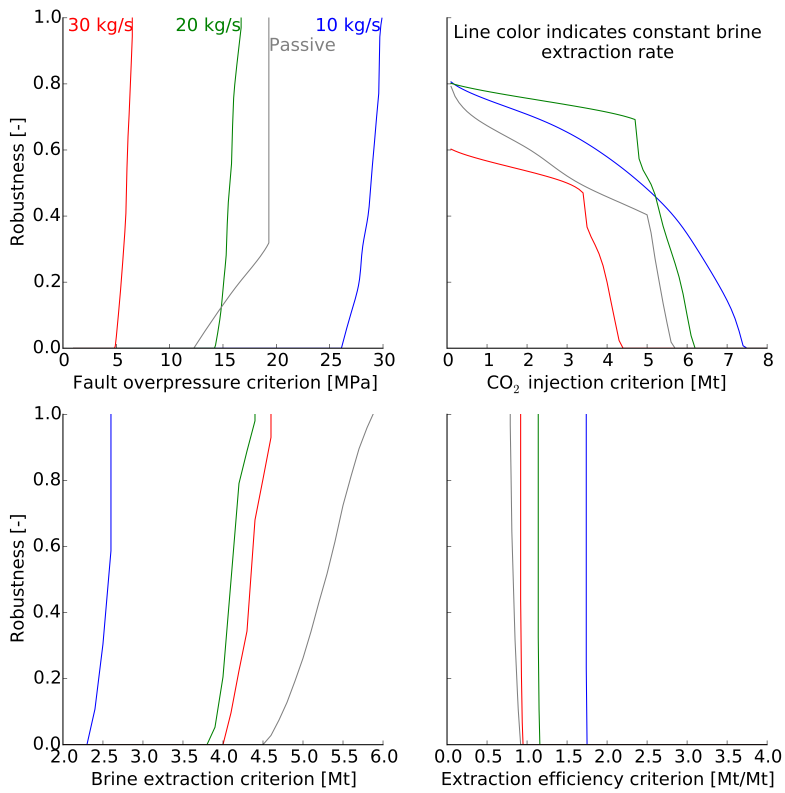

Figure 16: Single brine extraction well strategy comparing different constant brine extraction rates (indicated by line color) with the brine extraction well located at 1232 m from the CO_2 injection well. Robustness as a function of fault overpressure, CO_2 injection, brine extraction, and extraction efficiency is plotted.

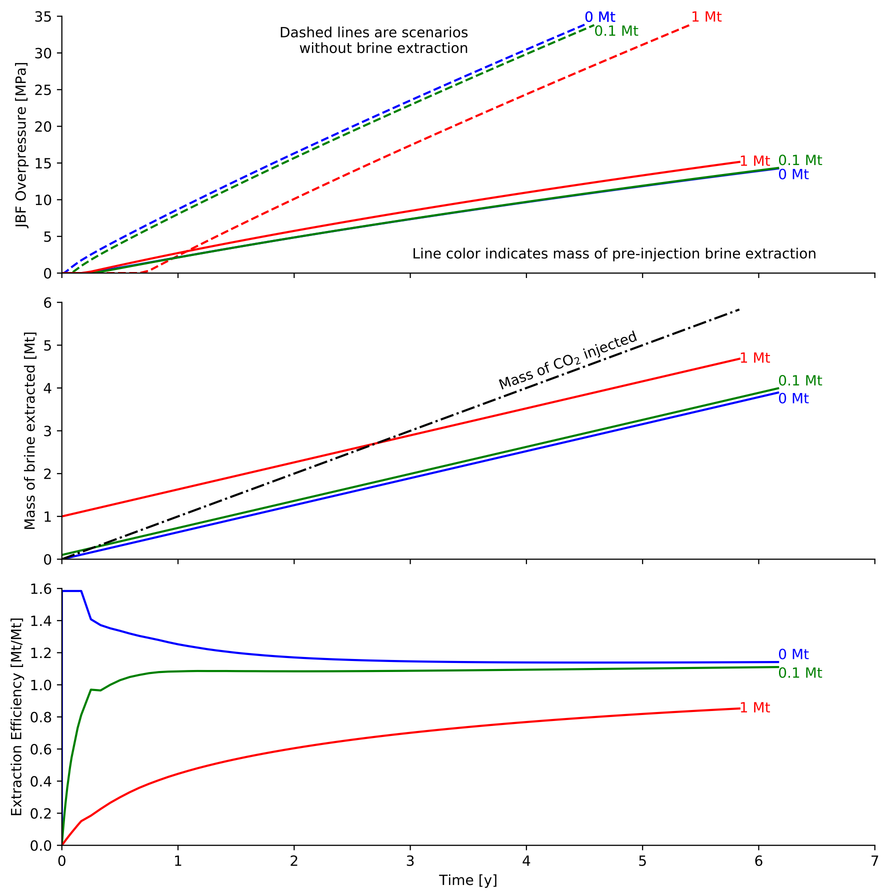

Figure 17: Single brine extraction well strategy with constant 20 kg/s brine extraction rate comparing different quantities of pre-injection brine extraction (indicated by line color) for the nominal permeability field. Time series of overpressure at the Jim Bridger Fault (JBF), mass of brine extracted, and extraction efficiency are plotted. The single brine extraction well is located 1232 m from the CO_2 injection well toward the Jim Bridger Fault.

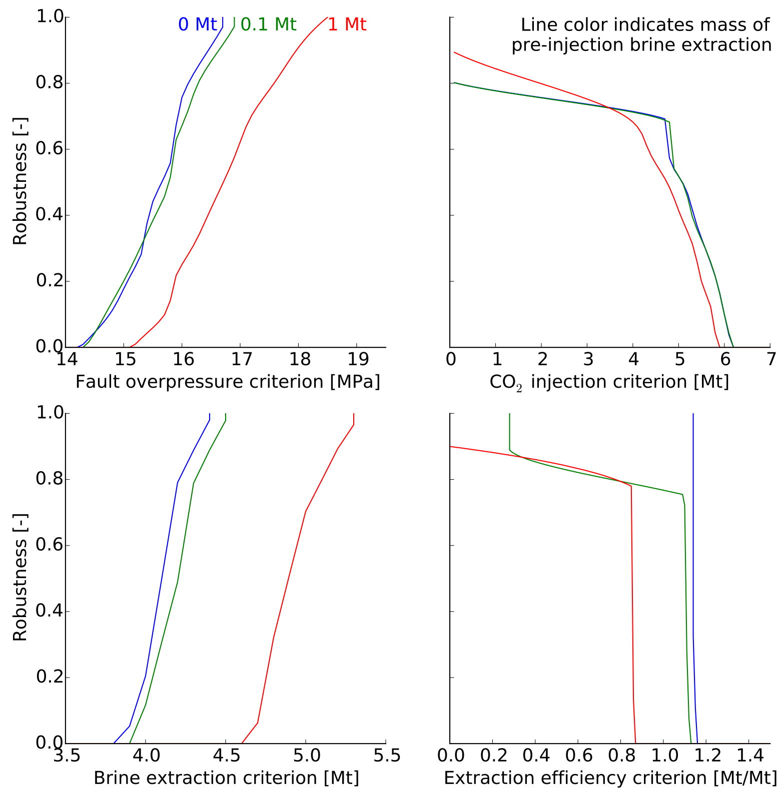

Figure 18: Single brine extraction well strategy with constant brine extraction rate of 20 kg/s comparing different pre-injection brine extraction quantities (indicated by line color) with the brine extraction well located at 1232 m from the CO_2 injection well toward the Jim Bridger Fault. Robustness as a function of fault overpressure, CO_2 injection, brine extraction, and extraction efficiency is plotted.

5. Discussion

We conducted a detailed evaluation and comparison of the robustness in achieving performance criteria for various pressure management strategies for geologic CO_2 injection for storage. Informing the selection of a pressure management strategy requires that threshold values for performance criteria be defined. To illustrate, we chose: $\mathrm{d}p_r^c = 20$ MPa, $m_c^c = 5$ Mt, $m_b^c = 7$ Mt, $e^c = 0.9$ These values were chosen to demonstrate the approach and are not intended to be taken as operational decisions for the RSUCSS. Using these threshold values, we compared alternative pressure management strategies according to the minimum criteria robustness (equation 17). Different threshold values may result in different conclusions about the preferred pressure management strategy. We present the comparison in Table 2. The comparison indicates in the first 8 rows of the far right column that non-zero overall robustness is achieved for the single passive extraction well strategy only when the brine extraction well is placed at 1232 m from the CO_2 injection well. Therefore, placing the well at the approximate midpoint between the CO_2 injection well and the fault is the most robust strategy in this analysis. The three passive extraction well strategies (rows 9-14) have very low overall robustness indicating that the expense of the additional wells does not provide increased overall robustness. The highest overall robustness ($\sim$0.52) occurs for constant rate brine extraction of 20 kg/s, either with 0.1 Mt (row 19) or no pre-injection brine extraction (rows 16 or 18). Since there are two cases with this overall robustness (three in the table, but two are duplicates presented for completeness in the figure associations in the first column), the individual criterion robustnesses can be used to further distinguish between strategies. A constant rate injection of 20 kg/s with no pre-injection brine extraction maximizes the overall robustness criteria. The conclusions drawn from this comparison are site specific, depend on designated criteria threshold values and are not necessarily generally applicable to all CO_2 injection locations. We demonstrated a formal decision analysis that can be used for potential geologic CO_2 storage sites. This decision analysis framework focuses on evaluating the robustness of achieving project performance criteria as opposed to optimizing the designs to exactly meet performance criteria.

This approach can be extended to an economic analysis by applying costs associated with the alternative strategies (well completion costs; pumping and treatment costs, active versus passive brine extraction, etc.). If extracted brine is re-injected as opposed to treated, modeling of the re-injection would have to be performed and additional performance criteria (similar to equations 8 through 11) and associated robustness metrics (similar to equations 13 through 16) defined and evaluated. For example, robustness against induced seismicity due to overpressurization from re-injection can be evaluated analogously to how overpressurization of the Jim Bridger fault was handled here (e.g., analogous performance criteria to equation 8 and robustness metric to equation 13). This approach could also be applied to a post mortem analysis of a real injection site, such as In Salah, which was shut down due to unexpected migration of CO2 (White et al., 2014).

Table 2: Individual criteria and overall minimum robustness of pressure management strategies. Performance criteria are set to fault overpressure less than 20 MPa, at least 5 Mt of CO_2 injected, less than 7 Mt of brine extracted and greater than 0.9 extraction efficiency. Robustness is truncated at 1 based on our sampling, while in theory it has no limit. Robustness values scale from red at zero to blue at one. Duplicate rows are included for completeness of figure associations in the first column.

Figures	Distance from injector [-]	Number of extractors [m]	Pre-injection brine extraction [Mt]	Brine extraction rate [kg/s]	Robustness: Fault overpressure ($\mathrm{d}p_r^c = 20$ MPa)	Robustness: CO_2 injection ($m_c^c = 5$ Mt)	Robustness: Brine extraction ($m_b^c = 7$ Mt)	Robustness: Extraction efficiency ($e^c = 0.9$)	Minimum Robustness
6,7,8	474	1	0	Passive	1.000	0.000	1.000	0.306	0.000
	853	1	0	Passive	1.000	0.000	1.000	0.042	0.000
	1232	1	0	Passive	1.000	0.404	1.000	0.069	0.069
	1611	1	0	Passive	0.158	0.324	0.000	0.000	0.000
	1990	1	0	Passive	0.000	0.224	0.000	0.000	0.000
9,10,S2	1232	1	0	Passive	1.000	0.404	1.000	0.069	0.069
	1232	1	0.1	Passive	1.000	0.471	1.000	0.385	0.385
	1232	1	1	Passive	1.000	0.200	1.000	0.155	0.155
11,12,S3	474	3	0	Passive	0.208	1.000	0.044	0.254	0.044
	853	3	0	Passive	0.194	1.000	0.000	0.262	0.000
	1232	3	0	Passive	0.168	1.000	0.000	0.202	0.000
13,14,S4	853	3	0	Passive	0.194	1.000	0.000	0.262	0.000
	853	3	0.1	Passive	0.215	1.000	0.000	0.462	0.000
	853	3	1	Passive	0.000	1.000	0.000	0.480	0.000
15,16,S5	1232	1	0	10	0.000	0.482	1.000	1.000	0.000
	1232	1	0	20	1.000	0.518	1.000	1.000	0.518
	1232	1	0	30	1.000	0.000	1.000	1.000	0.000
17,18,S6	1232	1	0	20	1.000	0.518	1.000	1.000	0.518
	1232	1	.1	20	1.000	0.519	1.000	0.781	0.519
	1232	1	1	20	1.000	0.415	1.000	0.000	0.000

6. Conclusions

In this paper, we present a new approach to selecting pressure management strategies based on concepts from information gap theory. The approach focuses on evaluating the robustness against multiple performance criteria, including not exceeding fault overpressure, failing to inject a desired quantity of CO_2, not extracting more brine than desired, and failing to achieve an extraction efficiency. Our approach allows for a detailed evaluation and comparison of competing and complimentary performance criteria while taking into account uncertainties. While we present results that consider uncertainty in permeability, our approach can be used to assess the effect of uncertainties in multiple parameters. The approach provides an alternative to optimization strategies which identify solutions that exactly meet specified criteria without a detailed consideration of strategy robustness. Considering performance criteria robustness is critically important for applications like CO_2 sequestration, where site characterization is expensive, data are sparse given the depths of target reservoirs, and where stakes can be high with respect to policy support and public opinion.

Acknowledgments

We are grateful for support from the Brine Extraction Storage Test Project funded by the United States Department of Energy (DE-FE0026159); the United States Department of Energy Fossil Energy Office through the National Risk Assessment Partnership (NRAP) managed by the National Energy Technology Laboratory (NETL); and the US-China Advanced Coal

Technology Consortium (under management of West Virginia University). K.A.H., J.M.B., and R.S.M. thank the United States Department of Energy for a Mickey Leland Fellowship that was awarded to K.A.H. Computer clusters at Los Alamos National Laboratory supported by the Los Alamos National Laboratory High Performance Computing Environments Group were utilized during this research.

Bacon, D. H., Qafoku, N. P., Dai, Z., Keating, E. H., Brown, C. F., 2016. Modeling the impact of carbon dioxide leakage into an unconfined, oxidizing carbonate aquifer. International Journal of Greenhouse Gas Control 44, 290–299.

Ben-Haim, Y., 2006. Info-gap decision theory: decisions under severe uncertainty. Academic Press.

Benson, S. M., Cole, D. R., 2008. Co2 sequestration in deep sedimentary formations. Elements 4 (5), 325–331.

Berger, J. O., 2013. Statistical decision theory and Bayesian analysis. Springer Science & Business Media.

Berger, J. O., Moreno, E., Pericchi, L. R., Bayarri, M. J., Bernardo, J. M., Cano, J. A., De la Horra, J., Martín, J., Ríos-Insúa, D., Betrò, B., et al., 1994. An overview of robust bayesian analysis. Test 3 (1), 5–124.

Bielicki, J. M., Pollak, M. F., Deng, H., Wilson, E. J., Fitts, J. P., Peters, C. A., 2016. The leakage risk monetization model for geologic co2 storage. Environmental science & technology 50 (10), 4923–4931.

Bielicki, J. M., Pollak, M. F., Fitts, J. P., Peters, C. A., Wilson, E. J., 2014. Causes and financial consequences of geologic co 2 storage reservoir leakage and interference with other subsurface resources. International Journal of Greenhouse Gas Control 20, 272–284.

Birkholzer, J. T., Cihan, A., Zhou, Q., 2012. Impact-driven pressure management via targeted brine extractionconceptual studies of co 2 storage in saline formations. International Journal of Greenhouse Gas Control 7, 168–180.

Birkholzer, J. T., Zhou, Q., 2009. Basin-scale hydrogeologic impacts of co 2 storage: capacity and regulatory implications. International Journal of Greenhouse Gas Control 3 (6), 745–756.

Buscheck, T. A., Bielicki, J. M., White, J. A., Sun, Y., Hao, Y., Bourcier, W. L., Carroll, S. A., Aines, R. D., 2016a. Pre-injection brine production in CO_2 storage reservoirs: an approach to augment the development, operation, and performance of ccs while generating water. International Journal of Greenhouse Gas Control 54, 499–512.

Buscheck, T. A., Sun, Y., Hao, Y., Wolery, T. J., Bourcier, W., Tompson, A. F. B., Jones, E. D., Julio Friedmann, S., Aines, R. D., 2011. Combining brine extraction, desalination, and residual-brine reinjection with CO2 storage in saline formations: Implications for pressure management, capacity, and risk mitigation. Energy Procedia 4, 4283–4290.
URL http://dx.doi.org/10.1016/j.egypro.2011.02.378

Buscheck, T. A., White, J. A., Carroll, S. A., Bielicki, J. M., Aines, R. D.,

2016b. Managing geologic CO2 storage with pre-injection brine production: a strategy evaluated with a model of CO2 injection at Snohvit. Energy Environ. Sci.
URL http://dx.doi.org/10.1039/c5ee03648h

Cappa, F., Rutqvist, J., 2011. Impact of co2 geological sequestration on the nucleation of earthquakes. Geophysical Research Letters 38 (17).

Carey, J. W., Svec, R., Grigg, R., Zhang, J., Crow, W., 2010. Experimental investigation of wellbore integrity and co 2–brine flow along the casing–cement microannulus. International Journal of Greenhouse Gas Control 4 (2), 272–282.

Clarey, K., Thompson, M., 2010. Chapter 2, Study Area. In: Copeland D, Ewald E (eds) Available groundwater determination technical memorandum, Green River Basin Water Plan II. Report to the Wyoming Water Development Commission by the Wyoming State Geological Survey et al., 1–36.

Curry, T. E., Reiner, D. M., Ansolabehere, S., Herzog, H., 2005. How aware is the public of carbon capture and storage? MIT.

Davies, R. J., 2011. Methane contamination of drinking water caused by hydraulic fracturing remains unproven. Proceedings of the National Academy of Sciences 108 (43), E871–E871.

Dempsey, D., Kelkar, S., Pawar, R., Keating, E., Coblentz, D., 2014. Modeling caprock bending stresses and their potential for induced seismicity during co 2 injection. International Journal of Greenhouse Gas Control 22, 223–236.

Deng, H., Stauffer, P. H., Dai, Z., Jiao, Z., Surdam, R. C., 2012. Simulation of industrial-scale co 2 storage: Multi-scale heterogeneity and its impacts on storage capacity, injectivity and leakage. International Journal of Greenhouse Gas Control 10, 397–418.

Elliot, T. R., Dammel, J., Buscheck, T. A., Rohmer, J., Celia, M. A., et al., 2012. Promising synergies to address water, sequestration, legal, and public acceptance issues associated with large-scale implementation of co2 sequestration. Mitigation and Adaptation Strategies for Global Change 17 (6), 569–599.

Ellsworth, W. L., 2013. Injection-induced earthquakes. Science 341 (6142), 1225942.

EPA, U. S., 2016. Hydraulic Fracturing for Oil and Gas: Impacts from the Hydraulic Fracturing Water Cycle on Drinking Water Resources in the United States (Final Report). Tech. rep., U.S. Environmental Protection Agency, Washington, DC.

Giardini, D., 2009. Geothermal quake risks must be faced. Nature 462 (7275), 848–849.

Harp, D. R., Pawar, R., Carey, J. W., Gable, C. W., 2016. Reduced order models of transient co 2 and brine leakage along abandoned wellbores from geologic carbon sequestration reservoirs. International Journal of Greenhouse Gas Control 45, 150–162.

Harp, D. R., Vesselinov, V. V., 2013. Contaminant remediation decision analysis using information gap theory. Stochastic environmental research and risk assessment 27 (1), 159–168.

Huerta, N. J., Hesse, M. A., Bryant, S. L., Strazisar, B. R., Lopano, C. L., 2012. Experimental evidence for self-limiting reactive flow through a fractured cement core: Implications for time-dependent wellbore leakage. Environmental science & technology 47 (1), 269–275.

Jordan, A. B., Stauffer, P. H., Harp, D., Carey, J. W., Pawar, R. J., 2015. A response surface model to predict co 2 and brine leakage along cemented wellbores. International Journal of Greenhouse Gas Control 33, 27–39.

Keating, E. H., Fessenden, J., Kanjorski, N., Koning, D. J., Pawar, R., 2010. The impact of co2 on shallow groundwater chemistry: observations at a natural analog site and implications for carbon sequestration. Environmental Earth Sciences 60 (3), 521–536.

Keating, E. H., Harp, D. H., Dai, Z., Pawar, R. J., 2016. Reduced order models for assessing co 2 impacts in shallow unconfined aquifers. International Journal of Greenhouse Gas Control 46, 187–196.

Keranen, K. M., Weingarten, M., Abers, G. A., Bekins, B. A., Ge, S., 2014. Sharp increase in central oklahoma seismicity since 2008 induced by massive wastewater injection. Science 345 (6195), 448–451.

Lewicki, J., Oldenburg, C., Dobeck, L., Spangler, L., 2007a. Surface co2 leakage during two shallow subsurface co2 releases. Geophysical Research Letters 34 (24).

Lewicki, J. L., Birkholzer, J., Tsang, C.-F., 2007b. Natural and industrial analogues for leakage of co2 from storage reservoirs: identification of features, events, and processes and lessons learned. Environmental Geology 52 (3), 457–467.

Little, M. G., Jackson, R. B., 2010. Potential impacts of leakage from deep co2 geosequestration on overlying freshwater aquifers. Environmental science & technology 44 (23), 9225–9232.

Lucier, A., Zoback, M., Gupta, N., Ramakrishnan, T., 2006. Geomechanical aspects of co2 sequestration in a deep saline reservoir in the ohio river valley region. Environmental Geosciences 13 (2), 85–103.

Majer, E. L., Baria, R., Stark, M., Oates, S., Bommer, J., Smith, B., Asanuma, H., 2007. Induced seismicity associated with enhanced geothermal systems. Geothermics 36 (3), 185–222.

Middleton, R. S., Keating, G. N., Stauffer, P. H., Jordan, A. B., Viswanathan, H. S., Kang, Q. J., Carey, J. W., Mulkey, M. L., Sullivan, E. J., Chu, S. P., et al., 2012. The cross-scale science of co 2 capture and storage: from pore scale to regional scale. Energy & Environmental Science 5 (6), 7328–7345.

Miller, E., Bell, L. M., Buys, L., 2007. Public understanding of carbon sequestration in australia: Socio-demographic predictors of knowledge, engagement and trust. International Journal of Emerging Technologies and Society 5 (1), 15–33.

Mukuhira, Y., Asanuma, H., Niitsuma, H., Häring, M. O., 2013. Characteristics of large-magnitude microseismic events recorded during and after stimulation of a geothermal reservoir at basel, switzerland. Geothermics 45, 1–17.

Navarre-Sitchler, A. K., Maxwell, R. M., Siirila, E. R., Hammond, G. E., Lichtner, P. C., 2013. Elucidating geochemical response of shallow heterogeneous aquifers to co 2 leakage using high-performance computing: implications for monitoring of co 2 sequestration. Advances in Water Resources 53, 45–55.

Nicot, J.-P., Hosseini, S. A., Solano, S. V., 2011. Are single-phase flow numerical models sufficient to estimate pressure distribution in co2 sequestration projects? Energy Procedia 4, 3919–3926.

Nordbotten, J. M., Kavetski, D., Celia, M. A., Bachu, S., 2008. Model for co2 leakage including multiple geological layers and multiple leaky wells. Environmental science & technology 43 (3), 743–749.

O'Malley, D., Vesselinov, V., 2015. Bayesian-information-gap decision theory with an application to co2 sequestration. Water Resources Research 51 (9), 7080–7089.

Osborn, S. G., Vengosh, A., Warner, N. R., Jackson, R. B., 2011. Methane contamination of drinking water accompanying gas-well drilling and hydraulic fracturing. Proceedings of the National Academy of Sciences 108 (20), 8172–8176.

Palmgren, C. R., Morgan, M. G., Bruine de Bruin, W., Keith, D. W., 2004. Initial public perceptions of deep geological and oceanic disposal of carbon dioxide. Environmental Science & Technology 38 (24), 6441–6450.

Pruess, K., 2008. On co2 fluid flow and heat transfer behavior in the subsurface, following leakage from a geologic storage reservoir. Environmental Geology 54 (8), 1677–1686.

Sminchak, J., Gupta, N., Byrer, C., Bergman, P., 2002. Issues related to seismic activity induced by the injection of co2 in deep saline aquifers. Journal of Energy & Environmental Research 2, 32–46.

Stauffer, P. H., Keating, G. N., Middleton, R. S., Viswanathan, H. S., Berchtold, K. A., Singh, R. P., Pawar, R. J., Mancino, A., 2011. Greening coal: breakthroughs and challenges in carbon capture and storage. Environmental science & technology 45 (20), 8597–8604.

Stauffer, P. H., Surdam, R. C., Jiao, Z., Miller, T. A., Bentley, R. D., 2009. Combining geologic data and numerical modeling to improve estimates of the co2 sequestration potential of the rock springs uplift, wyoming. Energy Procedia 1 (1), 2717–2724.

Surdam, R. C., 2013. Geological CO_2 storage characterization: The key to deploying clean fossil energy technology. Springer Science & Business Media.

Surdam, R. C., Jiao, Z., 2007. The rock springs uplift: An outstanding geological co2 sequestration site in southwest wyoming.

Surdam, R. C., Jiao, Z., Stauffer, P., Miller, T., 2009. An integrated strategy for carbon management combining geological co2 sequestration, displaced fluid production, and water treatment.

Thiem, G., 1906. Hydrologische Methoden: Dissertation zur Erlangung der Wurde eines... JM Gebhardt.

Trautz, R. C., Pugh, J. D., Varadharajan, C., Zheng, L., Bianchi, M., Nico, P. S., Spycher, N. F., Newell, D. L., Esposito, R. A., Wu, Y., et al., 2012. Effect of dissolved co2 on a shallow groundwater system: A controlled release field experiment. Environmental science & technology 47 (1), 298–305.

Viswanathan, H. S., Pawar, R. J., Stauffer, P. H., Kaszuba, J. P., Carey, J. W., Olsen, S. C., Keating, G. N., Kavetski, D., Guthrie, G. D., 2008. Development of a hybrid process and system model for the assessment of wellbore leakage at a geologic co2 sequestration site. Environmental science & technology 42 (19), 7280–7286.

Watson, T. L., Bachu, S., et al., 2007. Evaluation of the potential for gas and co2 leakage along wellbores. In: E&P Environmental and Safety Conference. Society of Petroleum Engineers.

White, J. A., Chiaramonte, L., Ezzedine, S., Foxall, W., Hao, Y., Ramirez, A., McNab, W., 2014. Geomechanical behavior of the reservoir and caprock system at the in salah co2 storage project. Proceedings of the National Academy of Sciences 111 (24), 8747–8752.

Wilson, E. J., Morgan, M. G., Apt, J., Bonner, M., Bunting, C., Gode, J., Haszeldine, R. S., Jaeger, C. C., Keith, D. W., McCoy, S. T., et al., 2008. Regulating the geological sequestration of co2. Environmental Science & Technology 42 (8), 2718–2722.

Supplemental material

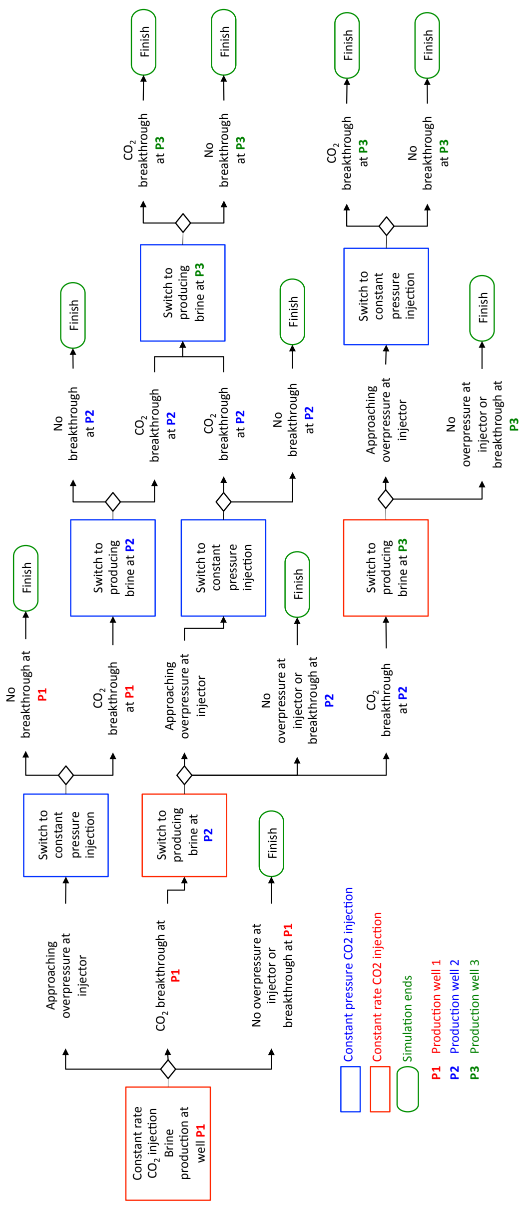

Figure S1: Triple brine extraction well pressure management simulation flow diagram illustrating injection and extraction operating decisions applied to FEHM simulations.

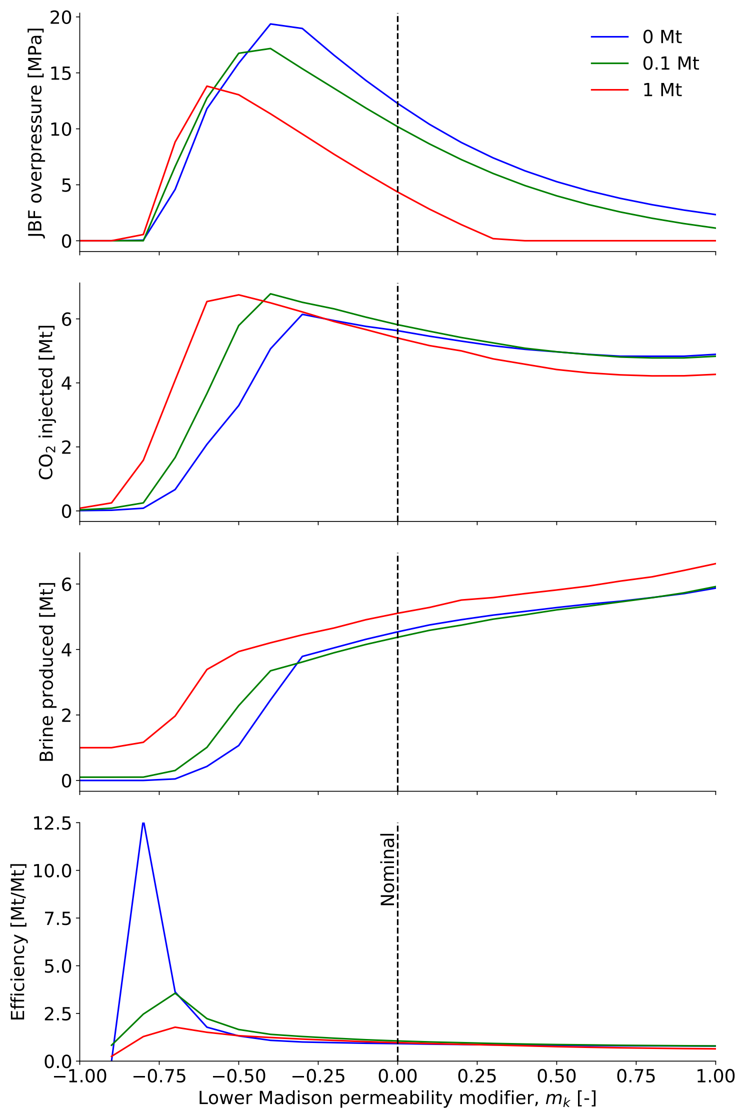

Figure S2: Jim Bridger Fault (JBF) overpressure, CO_2 injected, brine extracted, and extraction efficiency as a function of the permeability modifier for the single passive brine extraction well at 1232 m from the CO_2 injection well comparing different levels of pre-injection brine extraction.

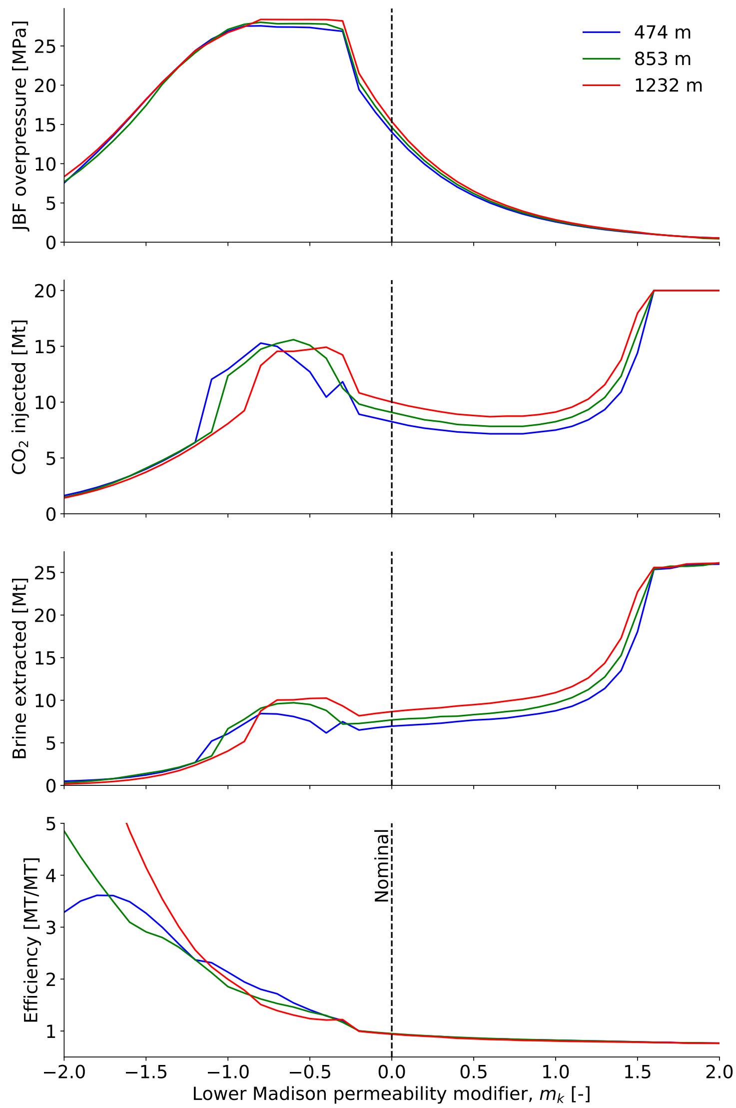

Figure S3: Jim Bridger Fault (JBF) overpressure, CO_2 injected, brine extracted, and extraction efficiency as a function of the permeability modifier for the three successive passive brine extraction wells comparing placing the first well at different distances from the CO_2 injection well. Successive wells are placed halfway between the preceding brine extraction well and the Jim Bridger Fault.

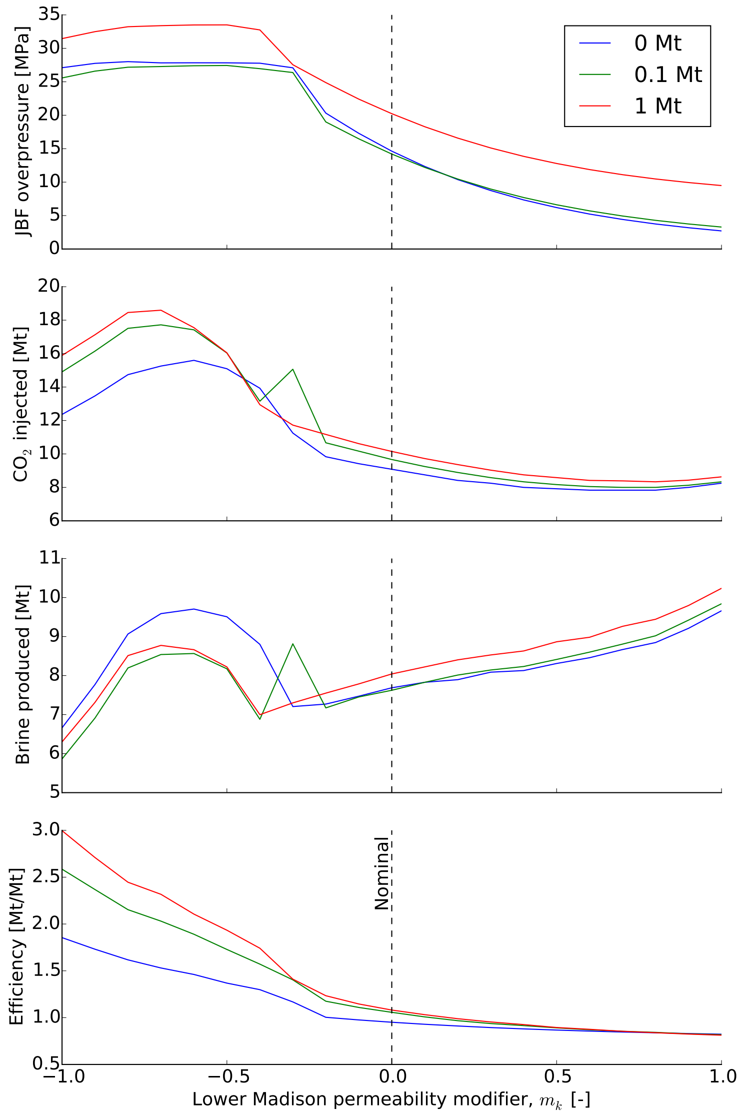

Figure S4: Jim Bridger Fault (JBF) overpressure, CO_2 injected, brine extracted, and extraction efficiency as a function of the permeability modifier for the three successive passive brine extraction wells with the first well located at *853 m* from the CO_2 injection well comparing different levels of pre-injection brine extraction. Successive wells are placed halfway between the preceding brine extraction well and the Jim Bridger Fault.

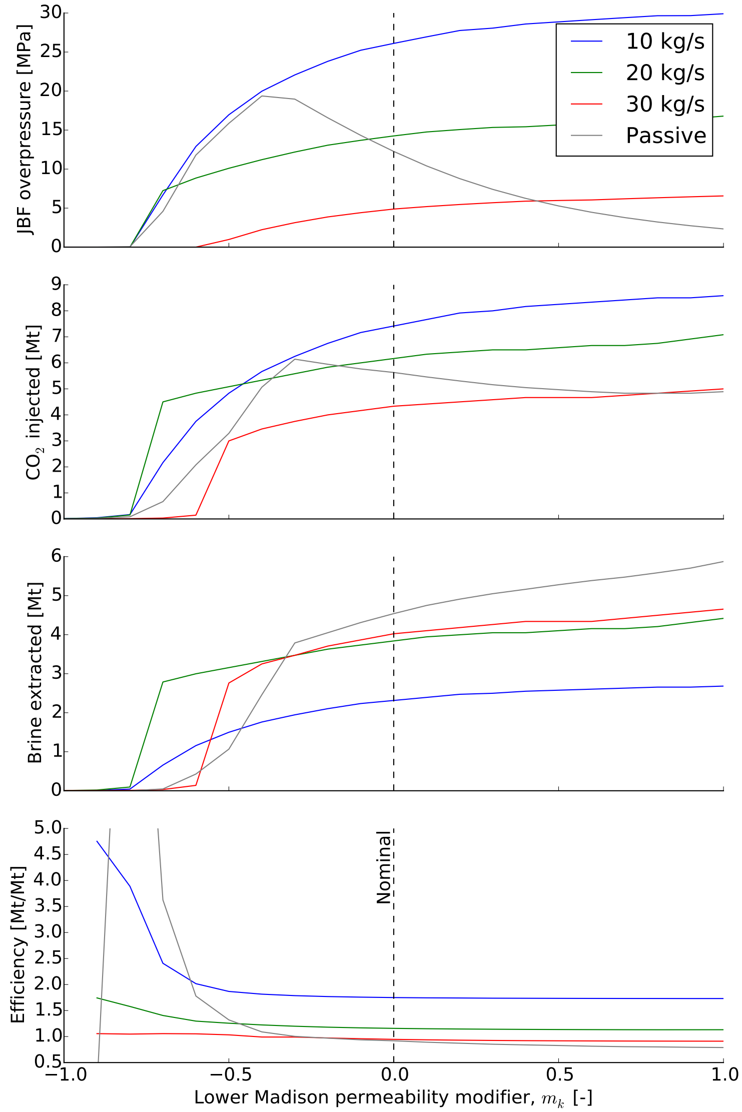

Figure S5: Jim Bridger Fault (JBF) overpressure, CO_2 injected, brine extracted, and extraction efficiency as a function of the permeability modifier for the single passive brine extraction well at 1232 m from the CO_2 injection well comparing different constant brine extraction rates. The associated passive extraction scenario is shown for reference in gray.

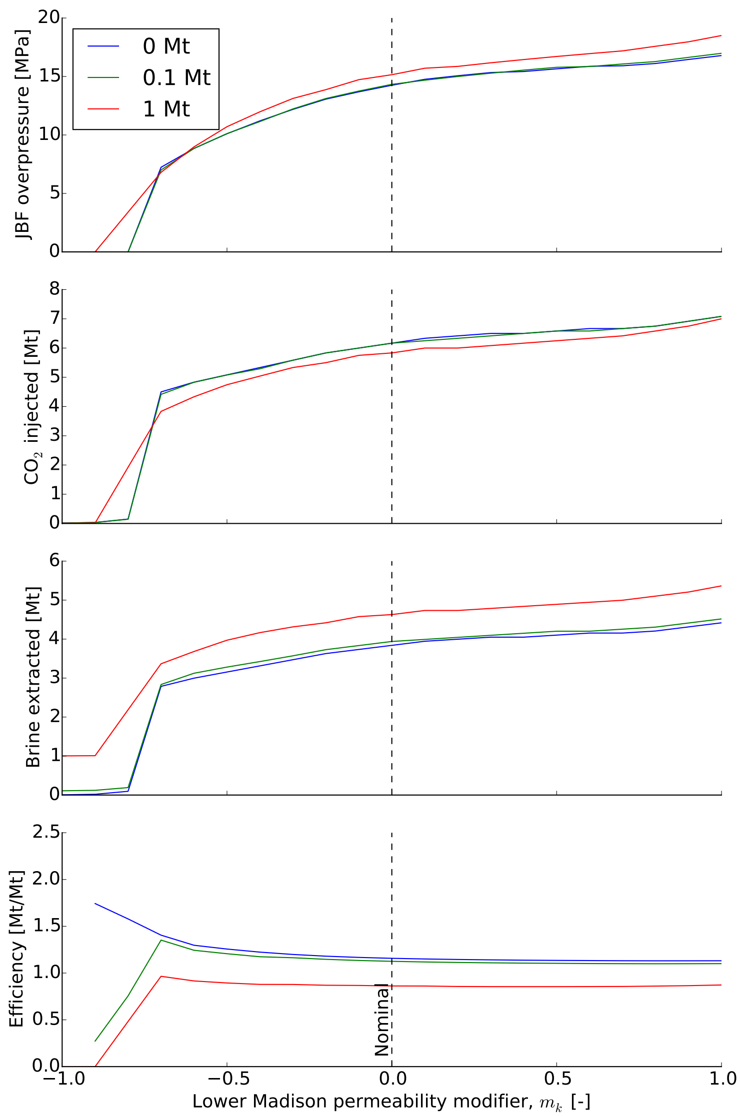

Figure S6: Jim Bridger Fault (JBF) overpressure, CO_2 injected, brine extracted, and extraction efficiency as a function of the permeability modifier for the single passive brine extraction well at 1232 m from the CO_2 injection well with 20kg/s constant brine extraction rate comparing different levels of pre-injection brine extraction.